R. & M. No. 3514

MINISTRY OF TECHNOLOGY

AERONAUTICAL RESEARCH COUNCIL
REPORTS AND MEMORANDA

A Theory of the Aerodynamic Interference between a Helicopter Rotor Blade and a Fuselage and Wing in Hovering and Forward Flight

By A. R. S. Bramwell, M.Sc., Ph.D.
with Appendix B on some Experimental Measurements
By J. B. B. Johnston, B.Sc.(Eng.)

LONDON: HER MAJESTY'S STATIONERY OFFICE
1968
PRICE £1 5*s.* 6*d.* NET

A Theory of the Aerodynamic Interference between a Helicopter Rotor Blade and a Fuselage and Wing in Hovering and Forward Flight

By A. R. S. Bramwell, M.Sc., Ph.D.
with Appendix B on some Experimental Measurements
By J. B. B. Johnston, B.Sc.(Eng.)

Reports and Memoranda No. 3514*
June, 1965

Summary.

The Report presents a theory of the aerodynamic interference between a helicopter rotor blade and a fuselage or wing. A two-dimensional analysis is made to which a correction factor is applied to convert the two-dimensional calculations to the appropriate three-dimensional case.

The pressures and forces on circular and square-sectioned fuselages and on wings are calculated for hovering flight and also the corresponding changes of lift on the blade. It is shown that large changes of blade lift occur if the blade is close to a fuselage due to the interference by the fuselage of the downwash or normal component of flow. The calculations also show that the interference effects on, and due to, a square sectioned fuselage are about half as large again as those of a circular cylinder whose diameter is the same as the length of the side of the square.

The analysis is extended to cover the case of interference between a blade and a lifting wing or tailfin in forward flight. It is shown that the interference between a tailfin and tailrotor can be severe and may result in a large loss of effectiveness of the tailrotor, especially in hovering and low speed flight.

LIST OF CONTENTS

*Replaces R.A.E. Tech. Report No. 65 127—A.R.C. 27 224.

LIST OF CONTENTS—*continued*

1. *Introduction.*

When a helicopter hovers the fuselage and other components, such as a wing or tailplane, are partially or wholly immersed in the rotor slipstream. Apart from the steady loads due to the rotor slipstream, it is known[1,2] that large transient loads occur as the blades pass over these surfaces and that these loads increase the nearer the surfaces are to the rotor. These loads are not only important because they may affect aerodynamic efficiency, but because they could also be a serious source of vibration. The proposals for helicopters with retractable rotors and other forms of high speed VTOL aircraft, which have rotors close to fuselages and wings, mean that this problem could become even more acute in the future. Further important interference effects are those which affect a tailrotor if close to a wide fuselage or fin.

Refs. 1 and 2 above, describe some measurements of periodic pressures on cylinders and flat plates under a rotor but so far there appear to have been no corresponding theoretical studies. The purpose of this Report is to provide such a study which will predict and explain the transient loads.

The calculations of this Report fall into three groups, namely:

(i) the pressures and forces on a fuselage due to the passage of a blade,

(ii) the change of lift on the blade due to the presence of the fuselage,

(iii) the changes of lift on a blade and wing in forward flight.

In calculating (i) two assumptions are made which greatly simplify the analysis. Firstly, the flow around the blade's aerofoil is replaced by line vortex flow, corresponding to the bound vortex of finite aerofoil theory. It is shown that this is a good approximation even when the blade is only a chord's distance from the fuselage. Secondly, the flow in any plane normal to the fuselage is assumed, at first, to be two-dimensional. This not only simplifies the calculation of the velocities and pressures but enables the methods of conformal transformation to be used to determine the flow about a variety of fuselage shapes. An approximation to three-dimensional flow is obtained by calculating an 'end effect' and applying it to the two-dimensional calculations mentioned above.

The fuselage cross-section shapes considered in this Report are the circle and square although the analysis can easily be extended to elliptical and rectangular sections. The calculation of (i) therefore is reduced mainly to the two-dimensional one of finding the velocities and pressures on a circle or square in the presence of a moving vortex.

In the initial calculations of (ii) the aerofoil flow is no longer assumed to be that of a simple vortex, except to approximate to its image in the fuselage and a flat-plate aerofoil is used to represent the blade. Actually, it is found that by far the most important effect is simply the local change of flow direction due to the interference of the downwash, or normal component of flow, by the fuselage.

In the calculation of (iii) we have to deal with the case in which two lifting surfaces are interfering with one another. If the rotor blade and wing are more than a chord distance from one another the simple vortex representation of the interfering lifting surface can be used. In cases where the blade and wing are very close, however, such as when a tailrotor is attached to a broad fin, it may be necessary to represent one or both of the lifting surfaces by two vortices, instead of one, as a better approximation.

Measurements of pressures on circular cylinders below a hovering rotor, have been made at R.A.E. and NASA, and pressure variations on a blade in the presence of a circular cylinder have been measured at R.A.E. For all these cases there is good agreement with the theory presented in this Report.

No attempt has been made to calculate the vibration due to aerodynamic interference.

2. *Calculation of Fuselage Pressures and Forces in Hovering Flight.*

2.1. *The Approximation to the Flow Around an Aerofoil.*

The flow around an aerofoil in the presence of a fuselage, both of arbitrary shape, is not only very complicated but, in general, no two-dimensional transformation exists which maps such a flow onto the $W = \Phi + i\psi$ plane. However, a great simplification can be made by replacing the flow around an aerofoil by the flow of a vortex having the same circulation. Milne-Thomson, in Ref. 3, calls this the 'substitution vortex'

and the justification for using it is as follows: The vortex flow, as seen by a stationary observer, will consist of a series of concentric circles. Now, the flow about the circle $|\zeta| = a$, in the ζ-plane, can be transformed into the flow about a flat-plate aerofoil of chord $c = 4a$, in the z-plane, by the transformation,

$$z = \zeta + \frac{a^2}{\zeta}. \tag{1}$$

It can be seen from (1) that as $|\zeta|$ increases the term $\frac{a^2}{\zeta}$ decreases and becomes negligible and the flow about the flat plate becomes more nearly like the flow in the ζ-plane, i.e. the vortex flow. The degree of approximation involved in taking $z = \zeta$ can be found by inverting (1) to obtain

$$\zeta = z - \frac{a^2}{z} - \ldots.$$

or, in terms of the flat-plate chord,

$$\frac{\zeta}{z} = 1 - \frac{c^2}{16z^2} - \ldots. \quad .$$

Putting $|z| = r$ gives $\left|\frac{c^2}{16z^2}\right| = \frac{c^2}{16r^2}$, so that if we take $r = c$, $\frac{c^2}{16r^2} = \frac{1}{16}$, which shows that the approximation $z = \zeta$ is quite good even at only a chord distance from the centre of the aerofoil. As we shall usually be concerned with distances at least as large as this, the error in assuming vortex flow in place of the aerofoil flow should be very small. A special case, in which the separation is smaller than this, is treated separately.

2.2. *Pressures and Forces on a Circular Fuselage.*

Although the velocity and circulation at a blade section vary along the blade and the fuselage cross-section may vary also, a two-dimensional analysis, described below, will be used to calculate the pressures and forces. It is found that for the constant section fuselage, at least, the two-dimensional approach is quite accurate up to a blade radius of about $0{\cdot}8R$ but, from that point outwards, the measured pressures fall off far more rapidly than the two-dimensional calculations predict. As will be seen in Section 2.5, this 'end effect' can be explained theoretically quite simply and the results then show good agreement with the measurements. An appropriate end correction will therefore be made to the two-dimensional calculations.

It will be assumed that the helicopter rear fuselage can be represented by an infinite circular cylinder of radius a, and that the flow around the blade aerofoil at a given point along its span, is that of an infinite line vortex having the local strength κ equal to $\frac{1}{2\pi}$ of the circulation about the blade's aerofoil.

We will take the centre of the circular fuselage as origin of co-ordinates and place the vortex at the point z_0, as in Fig. 1. If Ω is the angular velocity of the rotor and r is the radial distance of the section under consideration, $V = \Omega r$ is the speed with which the blade section passes the fuselage, i.e. the speed of the vortex relative to the chosen axes.

The image system of a vortex of strength κ at the point z_0 in the presence of a circular cylinder of radius a consists of a vortex of strength κ at the centre of the circle and another of strength $-\kappa$ at the inverse point $z = a^2/\bar{z}_0$. The complex potential of this system is then

$$W = i\kappa \log z + i\kappa \log (z - z_0) - i\kappa \log \left(z - \frac{a^2}{\bar{z}_0}\right). \tag{2}$$

In addition the fuselage will be immersed in the downwash (assumed steady) of the rotor. This velocity can be obtained from Ref. 4 which gives the relationship between the induced velocity at a given radial position at the rotor and at a corresponding point vertically below. The induced velocity at the rotor will have to be found in any case when determining the value of κ from blade strip theory. Calling this local induced velocity U, where U will be a function r and z_0, the complex potential becomes

$$W = -iUz+iUa^2/z+i\kappa \log (z-z_0)-i\kappa \log \left(z-\frac{a^2}{\bar{z}_0}\right). \tag{3}$$

In writing down equation (3) we have assumed that the fuselage is in a uniform flow, whereas, as we have implied above, the induced velocity varies in a vertical direction. However, from the information given in Ref. 4, it appears that except, perhaps, at points very close to the rotor's edge, the induced velocity field is nearly uniform and the assumption should be a reasonable one. For the purposes of calculation we will assume that the appropriate velocity is the velocity at the centre of the fuselage.

The velocity components, u and v, relative to the x and y axes, are given by

$$-u+iv = \frac{dW}{dz} = -iU-iUa^2/z^2+ i\kappa/z+\frac{i\kappa}{z-z_0}-\frac{i\kappa}{z-a^2/\bar{z}_0}. \tag{4}$$

If we put $z = ae^{i\theta}$, $z_0 = a_0 e^{i\theta_0}$, $\bar{z}_0 = a_0 e^{-i\theta_0}$, the velocity components at a point $P(a,\theta)$ on the cylinder surface are given by

$$\begin{aligned} -u+iv &= -iU-iUe^{-2i\theta}+\frac{i\kappa}{a}e^{-i\theta}+\frac{i\kappa}{ae^{i\theta}-a_0e^{i\theta_0}}-\frac{i\kappa}{ae^{i\theta}-\frac{a^2}{a_0}e^{i\theta_0}} \\ &= -i\left\{U(1+e^{-2i\theta})-\frac{\kappa}{a}e^{-i\theta}\left[1+\frac{1}{1-\frac{1}{k}e^{-i(\theta-\theta_0)}}-\frac{1}{1-ke^{-i(\theta-\theta_0)}}\right]\right\} \end{aligned}$$

where $k = a/a_0$ and

$$u+iv = -i\left\{U(1+e^{2i\theta})-\frac{\kappa}{a}e^{i\theta}\left[1+\frac{1}{1-\frac{1}{k}e^{i(\theta-\theta_0)}}-\frac{1}{1-ke^{i(\theta-\theta_0)}}\right]\right\}.$$

If the velocity at any point on the cylinder is q, we have

$$q^2 = (u-iv)(u+iv),$$

which after simplification becomes

$$q^2 = 4\left\{U\cos\theta-\frac{\kappa}{a_0}\frac{[k-\cos(\theta-\theta_0)]}{1-2k\cos(\theta-\theta_0)+k^2}\right\}^2. \tag{5}$$

Now, since the flow is unsteady, the appropriate form of Bernoulli's equation is

$$p+\tfrac{1}{2}\rho q^2-\frac{\partial\varphi}{\partial t} = p_0+\tfrac{1}{2}\rho U^2$$

where p_0 is the atmospheric pressure. To find $\frac{\partial \varphi}{\partial t}$ we must calculate the real part of $\frac{\partial W}{\partial t}$, so that differentiating (3) with respect to t, assuming κ constant, we get

$$\begin{aligned}\frac{\partial W}{\partial t} &= -\frac{i\kappa}{z-z_0}\frac{\partial z_0}{\partial t} - \frac{i\kappa}{z-a^2/\bar{z}_0}\cdot\frac{a^2}{\bar{z}_0^2}\frac{\partial \bar{z}_0}{\partial t} \\ &= -i\kappa\left\{\frac{1}{z-z_0}+\frac{a^2}{z\bar{z}_0^2-a^2\,\bar{z}_0}\right\}\frac{\partial z_0}{\partial t} \\ &= -i\kappa\ V\left\{\frac{1}{z-z_0}+\frac{a^2}{z\bar{z}_0^2-a^2\,\bar{z}_0}\right\} \qquad (6)\end{aligned}$$

since $$\frac{\partial z}{\partial t} = 0 \quad \text{and} \quad \frac{\partial z_0}{\partial t} = \frac{\partial \bar{z}_0}{\partial t} = \frac{\partial x_0}{\partial t} = V.$$

It is shown in Section 3.2 that, unless the blade is very close to the fuselage, the vortex strength κ varies little as it passes over the fuselage. Even when the blade is close to the fuselage, the most important case is the one in which the blade is directly above it, when κ is at a maximum and $\partial\kappa/\partial t$ is then zero. Thus the assumption of constant κ, in arriving at $\partial\varphi/\partial t$ would appear to be justified.

To find $\partial\varphi/\partial t$ on the cylinder we put $z = ae^{i\theta}$ and $z_0 = a_0 e^{i\theta_0}$ in (6) and obtain

$$\begin{aligned}\frac{\partial W}{\partial t} &= -i\,\kappa\,V\left\{\frac{1}{ae^{i\theta}-a_0e^{i\theta_0}}+\frac{1}{ae^{i\theta}-\frac{a^2}{a_0}e^{i\theta_0}}\cdot\frac{a^2\,e^{2i\theta_0}}{a_0^2}\right\} \\ &= -\frac{i\,\kappa\,V}{a_0}\left\{\frac{ke^{-i\theta}-e^{-i\theta_0}-k^2\,e^{i\theta_0}+ke^{-i\theta}\,e^{2i\theta_0}}{1-2k\cos(\theta-\theta_0)+k^2}\right\}\end{aligned}$$

and the real part is

$$\frac{\partial\varphi}{\partial t} = \frac{\kappa V}{a_0\{1-2k\cos(\theta-\theta_0)+k^2\}}\left[(1-k^2)\sin\theta_0 - 2k\cos\theta_0\sin(\theta-\theta_0)\right]. \qquad (7)$$

Thus the pressure at a point on the cylinder is

$$\begin{aligned}p-p_0 &= \rho\frac{\partial\varphi}{\partial t}+\tfrac{1}{2}\rho\,U^2-\tfrac{1}{2}\rho\,q^2 \\ &= \frac{\rho\,\kappa V}{a_0}\left[\frac{(1-k^2)\sin\theta_0-2k\cos\theta_0\sin(\theta-\theta_0)}{1-2k\cos(\theta-\theta_0)+k^2}\right]+ \\ &\quad +\tfrac{1}{2}\rho\,U^2-2\rho\left\{U\cos\theta-\frac{\kappa}{a_0}\frac{[k-\cos(\theta-\theta_0)]}{[1-2k\cos(\theta-\theta_0)+k^2]}\right\}^2. \qquad (8)\end{aligned}$$

We are more likely to be interested in the pressure increase, due to the passage of the blade, rather than the actual pressure. Thus, from (8) we must subtract the steady pressure $\frac{1}{2}\rho U^2(1-4\cos^2\theta)$ on the cylinder due to the downwash. The pressure increment then becomes

$$p-p_0' = \frac{\rho\kappa V}{a_0}\left[\frac{(1-k^2)\sin\theta_0 - 2k\cos\theta_0\sin(\theta-\theta_0)}{1-2k\cos(\theta-\theta_0)+k^2}\right] +$$

$$+\frac{2\rho\kappa}{a_0}\cdot\frac{k-\cos(\theta-\theta_0)}{1-2k\cos(\theta-\theta_0)+k^2}\left[2U\cos\theta-\frac{\kappa}{a_0}\cdot\frac{k-\cos(\theta-\theta_0)}{1-2k\cos(\theta-\theta_0)+k^2}\right] \tag{9}$$

where p_0' is the undisturbed pressure at the point of interest on the cylinder. In particular, if the blade is directly above the fuselage, $\theta_0 = \pi/2$ and

$$p-p_0' = \frac{\rho\kappa V}{a_0}\cdot\frac{1-k^2}{1-2k\sin\theta+k^2}+\frac{2\rho\kappa}{a_0}\cdot\frac{k-\sin\theta}{1-2k\sin\theta+k^2}\left[2U\cos\theta-\frac{\kappa}{a_0}\cdot\frac{k-\sin\theta}{1-2k\sin\theta+k^2}\right] \tag{10}$$

In terms of the local blade C_L, (10) can be written as

$$p-p_0' = \frac{\rho V^2 c C_L}{4\pi a_0(1-2k\sin\theta+k^2)}\left\{1-k^2+2(k-\sin\theta)\left(2v\cos\theta-\frac{c C_L}{4\pi a_0}\cdot\frac{k-\sin\theta}{1-2k\sin\theta+k^2}\right)\right\} \tag{11}$$

since $4\pi\kappa = Vc C_L$ and where $v = \dfrac{U}{V}$.

The pressures on a circular fuselage have been calculated, using equation (11), and are shown in Fig. 2 for the conditions stated. The lift coefficients of the blade have been calculated by the usual strip theory. At this stage, no account has been taken of the effect of the fuselage, on the circulation when the blade is close to the fuselage, as mentioned earlier, and no account has been taken of the 'end effect'. The calculations, shown in Fig. 2, show that by far the most important term is $\rho\dfrac{\partial\varphi}{\partial t}$, represented in equation (11) by the term multiplied by $1-k^2$. The remaining terms are seen to have a very small effect and could be neglected, especially when it appears that these pressure differences for points on either side of the vertical are almost equal and opposite, as shown by $\theta = 60$ deg and $\theta = 120$ deg in the lower diagram of Fig. 2, and would therefore cancel when the total force on the fuselage section was calculated. Thus a very good approximation to the pressure, when the blade is directly over the fuselage, is

$$p-p_0 = \rho\frac{\partial\varphi}{\partial t} = \frac{\rho V^2 c C_L}{4\pi a_0}\cdot\frac{1-k^2}{1-2k\sin\theta+k^2} \tag{12}$$

where we have returned to p_0 again since the above approximation implies that $p_0 = p_0'$.

For a general position of the blade

$$p-p_0 = \frac{\rho V^2 c C_L}{4\pi a_0} \cdot \left[\frac{(1-k^2)\sin\theta_0 - 2k\cos\theta_0 \sin(\theta-\theta_0)}{1-2k\cos(\theta-\theta_0)+k^2}\right] . \tag{13}$$

We can take $V = x\Omega R$, since the angle between the blade span and fuselage axis will be small for all cases of practical interest. For the calculation of the force per unit length of the fuselage, we will use the unsteady form of Blasius's theorem[5], which gives

$$X - i\,Y = \tfrac{1}{2} i \rho \int_c \left(\frac{\partial W}{\partial z}\right)^2 dz - i\rho \int_c \frac{\partial \overline{W}}{\partial t} d\bar{z} \tag{14}$$

where the contour of integration, c, encloses the cylinder but excludes the external vortex at z_0. The omission of the first integral of (14) corresponds to the approximation leading to equations (12) and (13), so that, neglecting this term and taking the conjugate of (14), we get

$$X + i\,Y = i\rho \int_c \frac{\partial W}{\partial t} dz$$

$$= \rho \kappa V \int_c \left\{\frac{1}{z-z_0} + \frac{a^2}{z-\frac{a^2}{\bar{z}_0}} \cdot \frac{1}{z_0^2}\right\} dz \tag{15}$$

from equation (6).

The only singularity of the integrand within the contour is at $z = \dfrac{a^2}{\bar{z}_0}$ and the residue of $\left(z - \dfrac{a^2}{\bar{z}_0}\right)^{-1}$ at $z = \dfrac{a^2}{\bar{z}_0}$ is unity.

Therefore

$$X + i\,Y = \frac{2\pi i \rho \kappa V a^2}{\bar{z}_0^2}$$

$$= 2\pi i \rho \kappa V k^2 (\cos 2\theta_0 + i \sin 2\theta_0)$$

and since $\kappa = \dfrac{V c C_L}{4\pi}$, we have

$$X = -\tfrac{1}{2} \rho V^2 c C_L k^2 \sin 2\theta_0 \tag{16}$$

and

$$Y = \tfrac{1}{2} \rho V^2 c C_L k^2 \cos 2\theta_0 . \tag{17}$$

These results check with the far more tedious method of integrating $(p-p_0)\cos\theta$ and $(p-p_0)\sin\theta$, in conjunction with equation (13) round the circle. It is interesting to note that if the blade has positive lift the cylinder is urged downwards whether the blade passes above or below the cylinder.

2.3. *Pressures and Forces on a Wing.*

In order to calculate the pressures and forces on a wing under a moving blade in the hovering condition we will represent the wing by a flat-plate aerofoil. We have already obtained the complex potential for a vortex in the presence of a cylinder and can obtain the corresponding potential for a flat plate by the transformation.

$$z = \zeta + \frac{a_1^2}{\zeta} \tag{1a}$$

where a_1 is the radius of the circle to be transformed into the flat plate. This circle is now in the ζ-plane, x,y axes are reserved, as usual, for the physical plane, as in Fig. 3.

It will simplify the calculations greatly to make the same approximation as in the previous section, i.e. of retaining only the $\rho \dfrac{\partial \varphi}{\partial t}$ term in estimating the pressure. We can therefore omit the downwash velocity altogether, since it makes no contribution to $\dfrac{\partial \varphi}{\partial t}$, and write, for the flow about the circle,

$$W = i\kappa \log \zeta + i\kappa \log (\zeta - \zeta_0) - i\kappa \log \left(\zeta - \frac{a_1^2}{\bar{\zeta}_0} \right)$$

where ζ_0 is the position of the blade vortex in the ζ-plane. Then

$$\frac{\partial W}{\partial t} = -i\kappa \left\{ \frac{1}{\zeta - \zeta_0} \frac{\partial \zeta_0}{\partial t} + \frac{1}{\zeta - \dfrac{a_1^2}{\bar{\zeta}_0}} \cdot \frac{a_1^2}{\bar{\zeta}_0^2} \cdot \frac{\partial \bar{\zeta}_0}{\partial t} \right\} . \tag{18}$$

Now
$$\frac{\partial \zeta_0}{\partial t} = \frac{\partial \zeta_0}{\partial z_0} \cdot \frac{\partial z_0}{\partial t} = V \frac{\partial \zeta_0}{\partial z_0}$$

and
$$\frac{\partial \bar{\zeta}_0}{\partial t} = \frac{\partial \bar{\zeta}_0}{\partial \bar{z}_0} \cdot \frac{\partial \bar{z}_0}{\partial t} = V \frac{\partial \bar{\zeta}_0}{\partial \bar{z}_0} \tag{19}$$

since, as before, $\dfrac{\partial z_0}{\partial t} = \dfrac{\partial \bar{z}_0}{\partial t} = V$.

Also, from (1*a*)

$$\frac{\partial \zeta_0}{\partial z_0} = \frac{\zeta_0^2}{\zeta_0^2 - a_1^2} \quad \text{and} \quad \frac{\partial \bar{\zeta}_0}{\partial \bar{z}_0} = \frac{\bar{\zeta}_0^2}{\bar{\zeta}_0^2 - a_1^2} . \tag{20}$$

Substituting the relations (19) and (20) into equation (18) gives

$$\frac{\partial W}{\partial t} = -i\kappa V \left\{ \frac{\zeta_0^2}{(\zeta - \zeta_0)(\zeta_0^2 - a_1^2)} + \frac{a_1^2}{\zeta - \dfrac{a_1^2}{\bar{\zeta}_0}} \cdot \frac{1}{\bar{\zeta}_0^2 - a_1^2} \right\} . \tag{21}$$

Points on the plate are represented by $\zeta = a_1 e^{i\chi}$ and the position of the blade by $\zeta_0 = a_0 e^{i\chi_0}$. Therefore the pressure on the plate is

$$p-p_0 = \text{Real part of } \rho \frac{\partial W}{\partial t}$$

$$= \text{Real part of } -i\rho\kappa V \left\{ \frac{a_0^2 e^{2i\chi_0}}{(a_1 e^{i\chi} - a_0 e^{i\chi_0})(a_0^2 e^{2i\chi_0} - a_1^2)} + \right.$$

$$\left. + \frac{a_1^2}{(a_1 e^{i\chi} - \frac{a_1^2}{a_0} e^{i\chi_0})(a_0^2 e^{-2i\chi_0} - a_1^2)} \right\}.$$

After some rearrangement and picking out the real part we find

$$p-p_0 = \frac{\rho\kappa V k'}{a_1} \frac{\{2k'(1-k'^2)\cos\chi_0 \sin(\chi_0-\chi)+(1-k'^4)\sin\chi_0\}}{\{1-2k'\cos(\chi-\chi_0)+k'^2\}\{1-2k'^2\cos 2\chi_0+k'^4\}}$$

$$= \frac{\rho V^2 c C_L k'}{\pi c_w} \frac{\{2k'(1-k'^2)\cos\chi_0 \sin(\chi_0-\chi)+(1-k'^4)\sin\chi_0\}}{\{1-2k'\cos(\chi-\chi_0)+k'^2\}\{1-2k'^2\cos 2\chi_0+k'^4\}} \tag{22}$$

where $k' = \frac{a_1}{a_0}$ and $c_w = 4a_1$ is the chord of the flat plate. The relationships between k' and χ and the co-ordinates x,y of the physical plane are given in Appendix A.
As in the previous case, the force components are most easily found by a contour integration, that is

$$X + iY = i\rho \int_c \frac{\partial W}{\partial t} dz = i\rho \int_\gamma \frac{\partial W}{\partial t} \frac{dz}{d\zeta}$$

where the contour of integration, γ, encloses the transforming cylinder but excludes the vortex at ζ_0.

Thus

$$X + iY = \rho\kappa V \int_\gamma \left\{ \frac{\zeta_0^2(\zeta^2-a_1^2)}{(\zeta-\zeta_0)(\zeta_0^2-a_1^2)\zeta^2} + \frac{a_1^2(\zeta^2-a_1^2)}{\left(\zeta-\frac{a_1^2}{\bar{\zeta}_c}\right)(\bar{\zeta}_0^2-a_1^2)\zeta^2} \right\} d\zeta .$$

The singularities within the contour are a double pole at $\zeta = 0$ and a simple pole at $\zeta = a_1^2/\bar{\zeta}_0$. Evaluating the residues at these singularities gives

$$X + iY = 2\pi i\rho\kappa V \left\{ \frac{a_1^2}{\zeta_0^2-a_1^2} + \frac{\bar{\zeta}_0^2}{\bar{\zeta}_0^2-a_1^2} - 1 \right\}$$

$$= \frac{2\pi i\rho\kappa V a_1^2\{(\zeta_0^2+\bar{\zeta}_0^2)-2a_1^2\}}{(\zeta_0^2-a_1^2)(\bar{\zeta}_0^2-a_1^2)} \tag{23}$$

from which we find

$$X = 0$$

$$Y = \tfrac{1}{2}\rho V^2 c C_L \left\{ \frac{2k'^2(\cos 2\chi_0 - k'^2)}{1 - 2k'^2 \cos 2\chi_0 + k'^4} \right\} . \tag{24}$$

The term outside the bracket in equation (24) is the local lift of the blade so that the term inside the bracket is the fraction of the blade lift transferred to the wing. As the blade approaches the wing $k' \to 1$ and the term in the bracket $\to -1$, that is, in the limit, all the lift of the blade is transferred to the wing, as we should expect.

2.4. *The Pressures and forces on a Fuselage of Square Section.*

In Section 2.2 the helicopter fuselage was typified by a circular cross-section. However, some recent helicopters, e.g. the Westland 'Rotodyne' and the Boeing-Vertol 'Chinok', have fuselages which are very nearly square and it would be interesting to find out how the pressures and forces on a square fuselage differ from a circular one. To do this we need the complex potential of a vortex in the presence of a square and this can be obtained by mapping the outside of the square onto the upper half of the τ-plane and placing a vortex pair in the τ-plane as shown in Fig. 4.

The complex potential of the vortex pair in the τ-plane is

$$W = i\kappa \log \frac{\tau - i b - V_\tau \Delta t}{\tau + i b - V_\tau \Delta t} \tag{25}$$

where b is the distance of either vortex from the $\sigma = 0$ axis and $V_\tau \Delta t$ is the horizontal distance travelled by the vortices in a short time Δt. Differentiating equation (25) with respect to time gives

$$\frac{\partial W}{\partial t} = -i\kappa V_\tau \left\{ \frac{1}{\tau - i b - V_\tau \Delta t} - \frac{1}{\tau + i b - V_\tau \Delta t} \right\} .$$

For the special case of $t = 0$, in which we shall be interested later, the vortices are at $\tau = \pm i b$, and therefore

$$\frac{\partial W}{\partial t} = \frac{2b\kappa V_\tau}{\tau^2 + b^2} . \tag{26}$$

A function which maps the outside of a rectangle onto the upper half of the τ-plane is

$$z = A \int_0^\tau \frac{\sqrt{(1-\tau^2)(k^2-\tau^2)}}{(k+\tau^2)^2} dt \tag{27}$$

where A fixes the scale and orientation of the rectangle and k is to be chosen so that the rectangle reduces to a square. Transformations of this type are discussed in Ref. 6.

Making the substitution $\tau = ksn(u,k)$ transforms (27) into

$$z = A \int_0^u \frac{cn^2 u\, dn^2 u}{(1 + k\, sn^2 u)^2} du$$

$$= \frac{A}{2k} \left[\frac{k\, sn\, u\, cn\, u\, dn\, u}{1 + k\, sn^2 u} - (1-k)u + E(u) \right] \tag{28}$$

where $E(u)$ is the elliptic integral of the second kind and $sn\ u$ etc. are Jacobian elliptic functions, all of modulus k. (This k, which is standard notation for elliptic functions, must not be confused with the k and k' of Sections 2.2 and 2.3.) Corresponding points in the τ-plane and z-plane are chosen to be

$$z = a, \qquad \tau = k, \qquad u = K \tag{29}$$

$$z = a-2ai, \qquad \tau = 1, \qquad u = K+iK' \tag{30}$$

where K and K' are complete elliptic integrals of the first kind of moduli k and $k'\left(=\sqrt{1-k^2}\right)$ respectively. Substituting the values from (29) into equation (28) gives

$$a = \frac{A}{2k}[E-(1-k)K] \tag{31a}$$

and the corresponding values of (30) give

$$a-2ai = \frac{A}{2k}[E+i(K'-E')-(1-k)(K+iK')] \tag{31b}$$

since $$dn(K+iK') = 0 \quad \text{and} \quad E(K+iK') = E+i(K'-E').$$

Subtracting (31*b*) from (31*a*) gives

$$a = \frac{A}{4k}(E'-kK'). \tag{32}$$

Hence, equations (31a) and (32) give us two relations for finding k and A.

From (31a) and (32)

$$2[E(k)-(1-k)K(k)] = E(k')-kK(k'). \tag{33}$$

Using the Gauss modulus transformation[7], we can write

$$E(k) = \frac{1}{1+\lambda}[E(\lambda')+\lambda K(\lambda')] \tag{34}$$

$$K(k) = \tfrac{1}{2}(1+\lambda)K(\lambda') \tag{35}$$

where $\lambda = \dfrac{1-k}{1+k}$ and $\lambda' = \sqrt{1-\lambda^2}$ and, since k is the same function of λ as λ is of k, we deduce from (34) and (35) that

$$E(k') = \frac{2}{1+\lambda}E(\lambda)-(1-\lambda)K(\lambda) \tag{36}$$

$$K(k') = (1+\lambda)K(\lambda). \tag{37}$$

Substituting the relations (34) to (37) into equation (33) gives

$$E(\lambda)-\lambda'^2 K(\lambda) = E(\lambda')-\lambda^2 K(\lambda)$$

which is clearly satisfied by taking $\lambda = \lambda' = 1/\sqrt{2}$ giving $k = 3-2\sqrt{2}$. Thus, by using the relations (34) to (37) we have been able to find the exact value of k instead of having to solve equation (33) by trial and error, or at any rate, by some approximate method. Either of equations (31) or (32) can now be used to find A and we obtain.

$$A = 1{\cdot}38334a$$

k and A having now been found, the transformation (27) is completely defined.

It will simplify calculations greatly to consider only the important case in which the blade is directly above the centre of the fuselage and assume that the way in which the pressures and forces vary with other (lateral) positions of the vortex is the same as for the circle for which the general case has been calculated [equations (12), (13), (16) and (17)].

The vortex in the τ-plane will lie on the imaginary axis, by symmetry. We now need a relationship between points on the imaginary axis in the τ-plane and corresponding points in the z-plane.

We already have $\tau = k\ sn(u,k)$, so that putting $\tau = i\,b$ and $u = i\,u_1$ say, we have, on using Jacobi's imaginary transformation,

$$\frac{sn\,(u_1, k')}{cn\,(u_1, k')} = \frac{b}{k}$$

from which

$$sn(u_1, k') = \frac{b}{\sqrt{b^2+k^2}} \tag{38}$$

$$cn(u_1, k') = \frac{k}{\sqrt{b^2+k^2}} \tag{39}$$

and

$$dn(u_1, k') = k\sqrt{\frac{1+b^2}{b^2+k^2}}. \tag{40}$$

Putting $i\,u_1$ for u equation (28) gives

$$z = \frac{Ai}{2k}\left[\frac{k\ sn(u_1, k')\,dn(u_1, k')}{cn(u_1, k')\,[cn^2(u_1, k') - k\ sn^2(u_1, k')]} - (1-k)\,u_1 + u_1 - E(u_1, k') + \frac{sn(u_1, k')\,dn(u_1, k')}{cn(u_1, k')}\right]$$

and using the relations (38) to (40), together with the familiar change of argument $\sin\varphi_1 \equiv sn(u_1, k') = b/\sqrt{b^2+k^2}$, gives finally

$$z = \frac{iA}{2}\left[\frac{b(1+k)}{k-b^2}\sqrt{\frac{1+b^2}{b^2+k^2}} + F(\varphi_1, k') - \frac{1}{k}E(\varphi_1, k')\right] \tag{41}$$

$$= i\,y_0, \text{ say}$$

A graph of y_0 against b is given in Fig. 5.

Now since τ is real on the boundaries of the square, equation (26) gives

$$\frac{\partial \varphi}{\partial t} = \frac{2b\,\kappa\,V_\tau}{\tau^2+b^2} \tag{42}$$

and

$$V_\tau = \frac{\partial \tau}{\partial t} = \frac{\partial \tau}{\partial z}\,\frac{\partial z}{\partial t} = \frac{V(k-b^2)^2}{A\sqrt{(1+b^2)\,(k^2+b^2)}} \tag{43}$$

when $\tau = i\,b$, i.e. the blade is over the middle of the fuselage. Also, the velocity, q, along the boundaries is

$$\begin{aligned} q &= \left|\frac{\partial W}{\partial z}\right| = \left|\frac{\partial W}{\partial \tau}\cdot\frac{\partial t}{\partial z}\right| \\ &= \left|\frac{2\,b\,\kappa}{\tau^2+b^2}\cdot\frac{(k+\tau^2)^2}{A\sqrt{(1-\tau^2)\,(k^2-\tau^2)}}\right| \end{aligned} \tag{44}$$

with the pressure difference being given, as before, by

$$p = \rho\frac{\partial \varphi}{\partial t} - \tfrac{1}{2}\rho\,q^2\,.$$

The pressure distribution round a square fuselage is shown in Fig. 6. The conditions are the same as for the cylinder of Fig. 2. (To simplify calculations for this case the coning angle has not been taken into account.) It can be seen that the pressures on the bottom of the fuselage are negligible and that therefore the force on the fuselage can be calculated by integrating the pressures on the top side only. It can also be seen from Fig. 6 that the effect of the $\frac{1}{2}\rho\,q^2$ term is small compared with $\rho\,\frac{\partial \varphi}{\partial t}$, as is the case with the circular cylinder, and will also be neglected in the calculation of the force on the fuselage.

The force on the fuselage is therefore

$$\begin{aligned} Y &= -\rho\int_{-a}^{+a}\frac{\partial \varphi}{\partial t}\,dz \\ &= -4\,\rho\,\kappa\,b\,V_\tau\int_0^k\frac{\partial \varphi}{\partial t}\,\frac{dz}{\partial t}\,d\tau \\ &= -4\,\rho\,\kappa\,b\,V_\tau\,A\int_0^k\frac{\sqrt{(1-\tau^2)\,(k^2-\tau^2)}\,d\tau}{(\tau^2+b^2)\,(k+\tau^2)^2}\,. \end{aligned} \tag{45}$$

$$Y = -\frac{4\,\rho\,\kappa\,V_\tau\,A}{b}\int_0^K\frac{cn^2\,u\,dn^2\,u\,du}{(1+\alpha^2\,sn^2\,u)\,(1+k\,sn^2\,u)^2}$$

or

$$\frac{Y}{\rho \kappa V} = -\frac{4(k-b^2)^2}{b\sqrt{(1+b^2)(k^2+b^2)}} \int_0^K \frac{cn^2\, u\, dn^2\, u\, du}{(1+\alpha^2\, sn^2\, u)(1+k\, sn^2\, u)^2}. \tag{46}$$

By partial fractions

$$\int_0^K \frac{cn^2\, u\, dn^2\, u\, du}{(1+\alpha^2\, sn^2\, u)(1+k\, sn^2\, u)^2} = \frac{\alpha^4}{(k-\alpha^2)^2} \int_0^K \frac{cn^2\ u\ dn^2\ u\ du}{1+\alpha^2\, sn^2\, u} -$$

$$-\frac{\alpha^2 k}{(k-\alpha^2)^2} \int_0^K \frac{cn^2\, u\, dn^2\, u\, du}{1+k\, sn^2\, u} + \frac{k}{k-\alpha^2} \int_0^K \frac{cn^2\, u\, dn^2\, u\, du}{(1+k\, sn^2\, u)^2}$$

$$= \frac{\alpha^4}{(k-\alpha^2)^2} I_1 - \frac{\alpha^2 k}{(k-\alpha^2)^2} I_2 + \frac{k}{k-\alpha^2} I_3, \text{ say.}$$

From Ref. 6

$$I_1 = \frac{1}{\alpha^4}[(1+\alpha^2)(k^2+\alpha^2)\,\Pi(K,-\alpha^2,k) - \alpha^2 E - (1+\alpha^2)k^2 K] \tag{47}$$

$$I_2 = \frac{1}{4k}[1+k)\pi - 4E + 2(1-k^2)K] \tag{48}$$

and

$$I_3 = \frac{1}{2k}[E-(1-k)K] \tag{49}$$

where $\Pi(K, -\alpha^2, k)$ is the complete elliptic integral of the third kind and is defined by $\Pi(K, -\alpha^2, k) = \int_0^u \frac{du}{1+\alpha^2\, sn^2\, u}$

From equations (46) and (41) and since $A = 1{\cdot}38334a$ it can be seen that $\frac{Y}{\rho \kappa V}$ is a function of $y_0/a = y$, say, only. This relationship is shown plotted in Fig. 7 together with the corresponding values for the circular cylinder from equation (17) ($\theta_0 = \pi/2$).

For the conditions given in Fig. 2 we find that the downward force on a square whose side is one foot is 9·75 lb per foot of fuselage. The corresponding force on a circular cylinder of one foot diameter is 6·35 lb per foot.

2.5. *Calculation of the 'End Effect'.*

So far we have calculated interference effects as if conditions were two-dimensional at each point along the blade. The trailing vortex sheet of the blade is assumed to have no effect on the interference (although it is taken account of in the estimation of the local C_L) and any vortex lines linking the image vortices (since they actually vary in strength) are assumed to be so short that they also make no contribution to the interference. Hence, the vortices producing interference are the finite line vortex of the blade and its images in the cylinder.

Now, the pressure on the fuselage, as can be seen from equation (13), is proportional to the product of the blade chord, C_L, and the square of the local blade velocity or, what is the same thing, the product of the circulation and the local blade velocity. In the special case of constant chord and incidence this product varies as the square of the radius of the blade element. As we shall see below, this simple variation enables a spanwise integration to be made quite easily and thus a comparison to be made between the two-dimensional analysis and one with finite vortices.

To find the relative contributions of the blade vortex and its images it is more convenient to refer to equation (6). $\frac{\partial W}{\partial t}$ is a measure of the air accelerations due to the changes of positions of the blade vortex and its image at the inverse of the circular cylinder. The term from the image at the cylinder centre is absent because it is stationery relative to the chosen axes system and cannot contribute to $\frac{\partial W}{\partial t}$ and therefore to $\frac{\partial \varphi}{\partial t}$. When typical values of z and z_0 are inserted into equation (6) it appears that the first term is several times larger than the second term. This is because the image vortex moves more slowly, relative to the cylinder, than the blade vortex and therefore the air accelerations due to the image vortex are correspondingly smaller. Hence, in order to get some idea of the 'end effect' it should be sufficient to consider only the blade vortex and assume that its strength is proportional to the radius of the blade element.

Referring to Fig. 8 and using the Biot-Savart law[3], the contribution to $\frac{\partial \varphi}{\partial t}$ at the point l of the cylinder, due to the vortex element $r\,dr$ is

$$d\left(\frac{\partial \varphi}{\partial t}\right) = \frac{hr^2\,dr}{\{(r-l)^2+h^2\}^{3/2}} \tag{50}$$

remembering that the blade velocity is proportional to r also.

The units are arbitrary since we shall be interested only in a ratio and not in absolute values.

Integrating equation (29) between $r = 0$ and $r = R$ gives

$$\frac{\partial \varphi}{\partial t} = h\int_0^R \frac{r^2\,dr}{\{(r-l)^2+h^2\}^{3/2}}$$

or

$$\frac{1}{h}\frac{\partial \varphi}{\partial t} = \sinh^{-1}\left(\frac{1-\varepsilon}{\gamma}\right)+\sinh^{-1}\left(\frac{\varepsilon}{\gamma}\right)-\frac{\left(1-\frac{\varepsilon^2}{\gamma^2}\right)+\varepsilon\left(1+\frac{\varepsilon^2}{\gamma^2}\right)}{\{(1-\varepsilon)^2+\gamma^2\}^{\frac{1}{2}}}+\frac{\varepsilon}{\gamma}\left(1+\frac{\varepsilon^2}{\gamma^2}\right)^{\frac{1}{2}}. \tag{51}$$

The corresponding two-dimensional analysis gives

$$\frac{1}{h}\frac{\partial \varphi}{\partial t} = 2\frac{\varepsilon^2}{\gamma^2}. \tag{52}$$

Generally, the blade chord and incidence will not be constant along the span but it will be assumed that the squared law variation of κV will represent most practical cases reasonably accurately.

The ratios, f, between the values of $\frac{\partial \varphi}{\partial t}$ calculated from equation (51) and equation (52) are shown in Fig. 9 for a range of γ. It is proposed that the pressures and forces for the three-dimensional case can be

obtained by extrapolating the two-dimensional values to about $\varepsilon = 1{\cdot}2$, say, and then multiplying them by f for the appropriate value of γ. This method has been applied to the two-dimensional values of Fig. 2 and the results are shown in Fig. 10 together with experimental values. It can be seen that the agreement is good.

3. *Forces on Rotor Blades in Hovering Flight.*

In the previous sections the calculations of the pressures and forces on circular and square fuselages were made possible by the approximation that the flow about the blade's aerofoil can be represented by the flow of a simple two-dimensional vortex. In order to calculate the effect of the presence of a circular cylinder on a lifting blade we will still suppose that the image of the blade flow in the cylinder is equivalent to two vortices, as in Section 2.2. Thus, as the blade moves over the cylinder, it will appear to the blade as if two vortices of opposite strength move relative to it at different speeds. The forces on the blade will arise from

(1) The unsteady flow corresponding to the terms $\rho \dfrac{\partial W}{\partial t}$.

(2) The change in the velocity field, and hence blade circulation, due to the presence of the fuselage in the neighbourhood of the aerofoil.

3.1. *Calculation of the Unsteady Forces on the Blade.*

The blade section will be represented by a flat-plate aerofoil. The image of its flow in a circular cylinder will be two vortices of equal and opposite strength at the centre of the cylinder and at the inverse point, as shown in Fig. 11. According to the approximation discussed in 2.1 the image vortices in the ζ-plane will be in the z-plane and their angular co-ordinates, as reckoned from the blade, will be the same. If the flat-plate is at incidence α, the complex potential for the flow about the aerofoil, of chord $c = 4a_1$, becomes

$$W(\zeta) = V\zeta\, e^{i\alpha} + \frac{Va_1^2}{\zeta} e^{-i\alpha} + i\kappa \log \zeta + i\kappa \log (\zeta - \zeta') - i\kappa \log \left(\zeta - \frac{a_1^2}{\bar{\zeta}'}\right) - i\kappa \log (\zeta - \zeta'') + i\kappa \log \left(\zeta - \frac{a_1^2}{\bar{\zeta}''}\right). \tag{53}$$

Now assuming κ remains constant, the first three terms are independent of time and we find that the calculation of $\dfrac{\partial W}{\partial t}$ becomes identical to that of Section 2.3, except that we are now dealing with two vortices instead of one. Thus to find the force on the blade arising from the unsteady terms we simply calculate Y by the method of Section 2.3 for the two vortices at $\zeta' = a_0' e^{i\chi_0}$ and $\zeta'' = a_0'' e^{i\chi_0}$.

As seen from the blade, the vortex at the centre of the cylinder moves with velocity $-V$ so that the contribution to Y from this vortex is

$$Y' = -\tfrac{1}{2}\rho V^2 c\, C_L \frac{\{2k'^2 (\cos 2\chi_0 - k'^2)\}}{1 - 2k'^2 \cos 2\chi_0 + k'^4}. \tag{54}$$

If a_0' is the distance of the vortex at the centre from the aerofoil, then the corresponding distance, a_0'', of the vortex at the inverse point is given by

$$a_0'' = a_0' - \frac{a^2}{a_0'} \tag{55}$$

and the velocity of this vortex relative to the blade is $-V\frac{a_0''}{a_0'}$. The unsteady force due to this vortex is then

$$Y'' = +\tfrac{1}{2}\rho V^2 c C_L \frac{a_0''}{a_0'} \frac{\{2k''^2(\cos 2\chi_0 - k''^2)\}}{(1-2k''^2\cos 2\chi_0 + k''^4)} \tag{56}$$

where
$$k' = \frac{a_1}{a_0'}$$

and
$$k'' = \frac{a_1}{a_0''} \tag{57}$$

Using the dimensions given in Fig. 2 and taking the case in which the blade is directly over the fuselage, $\chi_0 = -\frac{\pi}{2}$, we get $a_1 = 0{\cdot}125$, $a = 0{\cdot}5$, $a_0' = 1$, $a_0'' = 0{\cdot}75$, $k' = 0{\cdot}125$ and $k'' = 0{\cdot}1667$. Equations (54) and (56) then give

$$\frac{Y'}{\frac{1}{2}\rho V^2 c C_L} = 0{\cdot}0308$$

and

$$\frac{Y''}{\frac{1}{2}\rho V^2 c C_L} = -0{\cdot}0406$$

that is a loss of lift of about 1 per cent. Thus, even when the blade is only one chord width above the fuselage the change of lift due to the unsteady terms is negligibly small. It might be argued that with the aerofoil represented by a vortex the lift could be obtained from equation (15) of Section 2.2 by taking a contour which surrounds the vortex but excludes the cylinder. The only singularity in this contour is at $z = z_0$ and the integral is easily seen to be $2\pi i \rho V \kappa$, which is the steady lift on the blade. Thus the change of lift due to the unsteady pressures is zero but this is not inconsistent with the calculation above as the vortex corresponds to an aerofoil of vanishingly small chod, in which case, $k' = k'' = 0$ and hence $Y' = Y'' = 0$ also

3.2. *Calculation of the Change of Circulation due to the Presence of the Fuselage.*

To calculate this effect exactly would require a transformation which mapped the w-plane onto a flat plate, with a neighbouring circular cylinder, representing the fuselage, in the z-plane. Since such a transformation is not known we will use an approximate method of Milne-Thomson[3]. Milne-Thomson makes use of a theorem (Section 5·311 of Ref. 3) by which the circulation about a circular cylinder can be written down if the position of the stagnation point is given. The theorem states that if a point ζ_s is to be a stagnation point of the cylinder, and if the cylinder is placed in a flow whose complex potential is $f(\zeta)$, then the circulation about the cylinder is given by

$$2\pi K = 2\pi \times \text{real part of } 2i\zeta_s f'(\zeta_s). \tag{62}$$

Milne-Thomson uses this theorem to obtain an approximation to the mutual interference of a biplane (Section 8·7 of Ref. 3) by placing a vortex at the quarter-chord point of the lower wing, say, and replacing the upper wing by the circle which would transform it into an aerofoil. The theorem is then used to obtain the circulation about the transforming circle with the vortex of the lower wing and forward flight velocity providing the external flow whose complex potential is $f(\zeta)$. In our case the circle represents the blade and the vortex image system the external flow. Milne-Thomson's use of this theorem in calculating biplane interference implies that the positions of the image vortices in the physical and transformed planes are

the same and corresponds, therefore, to the approximation made in the previous Section. It will be convenient to split the relative velocity at the blade into the components U and V, i.e. perpendicular to and along the direction of blade motion. The blade chord makes an angle ϑ_0 (the collective pitch angle) with the direction of blade motion. For the complex potential we then have.

$$f(\zeta) = V\zeta e^{i\vartheta_0} - iU\zeta e^{i\vartheta_0} + \frac{ia^2 U e^{-i\vartheta_0}}{\zeta - \bar{\zeta}'} + i\kappa \log(\zeta - \zeta') - i\kappa \log(\zeta - \zeta'') \tag{63}$$

where $f(\zeta)$ is referred to axes fixed in the aerofoil circle, as in Fig. 11 (but with α replaced by V_0), ζ' is the position of the centre of the fuselage circle and $\zeta'' = \zeta' - a^2/\zeta'$.
Now U is small compared with V so that $U^2 + V^2 = V^2$ and, supposing ϑ_0 to be a small angle, we can absorb the second term of equation (63) into the first term and have approximately

$$f(\zeta) = V\zeta e^{i(\vartheta_0 - \nu)} + \frac{ia^2 U}{\zeta - \zeta'} + i\kappa \log(\zeta - \zeta') - i\kappa \log(\zeta - \zeta'') \tag{64}$$

$$\text{where } \nu = \frac{U}{V}.$$

Then

$$f'(\zeta) = Ve^{i(\vartheta_0 - \nu)} - \frac{ia^2 U}{(\zeta - \bar{\zeta}')^2} + \frac{i\kappa}{\zeta - \zeta'} - \frac{i\kappa}{\zeta - \zeta''}, \tag{65}$$

The stagnation point is at $\zeta = -a_1$, so that

$$-2ia_1 f'(-a_1) = -2ia_1 Ve^{i(\vartheta_0 - \nu)} - \frac{2a_1 a^2 U}{(a_1 + \bar{\zeta}')^2} - \frac{2a_1\kappa}{a_1 + \zeta'} + \frac{2a_1\kappa}{a_1 + \zeta''}. \tag{66}$$

It can be seen from Fig. 11 that, apart from the tilt of the blade due to the collective pitch angle ϑ_0, the blade will be directly over the fuselage when $\zeta' = -a_0' i$ and $\zeta'' = -a_0'' i$, and in this case

$$\begin{aligned} -2ia_1 f'(-a_1) &= -2ia_1 Ve^{i(\vartheta_0 - \nu)} - \frac{2a_1 a^2 U}{(a_1 + a_0' i)^2} - \frac{2a_1\kappa}{a_1 - a_0' i} + \frac{2a_1\kappa}{a_1 - a_0'' i} \\ &= -2ia_1 Ve^{i(\vartheta_0 - \nu)} - \frac{2a_1 a^2 U\{(a_1^2 - a_0'^2) - 2a_1 a_0' i\}}{a_1^4 + 2a_1^2 a_0'^2 + a_0'^4} - \\ &\quad - 2a_1\kappa\left\{\frac{a_1 + a_0' i}{a_1^2 + a_0'^2} - \frac{a + a_0'' i}{a_1^2 + a_0''^2}\right\} \end{aligned} \tag{67}$$

$$\text{where, as in 3.1., } a_0'' = a_0' - \frac{a^2}{a_0'}.$$

Then, from equation (62)
κ = real part of $-2ia_1 f(-a_1)$

$$= 2a_1 V \sin(\vartheta_0 - \nu) - \frac{2a_1 a^2 (a_1^2 - a_0'^2) U}{a_1^4 + 2a_1^2 a_0'^2 + a_0'^4} - 2a_1^2\kappa\left\{\frac{1}{a_1^2 + a_0'^2} - \frac{1}{a_1^2 + a_0''^2}\right\}$$

or

$$\kappa\left\{1+\frac{2a_1^2}{a_1^2+a_0'^2}-\frac{2a_1^2}{a_1^2+a_0''^2}\right\}=2a_1V\sin(\vartheta_0-\nu)-\frac{2a_1a^2(a_1^2-a_0'^2)U}{a_1^4+2a_1^2a_0'^2+a_0'^4} \tag{68}$$

Taking the same case as in 3.1., we find that the last two terms in the bracket on the left-hand side of equation (68) are negligible, being about 2 per cent of unity. Also, $a_1^2 << a_0'^2$, so that approximately

$$\kappa=2a_1V\left\{(\vartheta_0-\nu)+\nu\frac{a^2}{a_0'^2}\right\}. \tag{69}$$

If $2\pi\kappa_0$ is the steady undisturbed circulation, then

$$\kappa_0=2a_1V(\vartheta_0-\nu)$$

so that

$$\frac{\kappa}{\kappa_0}=1+\frac{\nu\dfrac{a^2}{a_0'^2}}{(\vartheta-\nu)}. \tag{70}$$

Now, by considering the flow about a circular cylinder in a uniform stream, it can easily be shown that if U is the velocity of the steady stream and U' is the local velocity upstream of the stagnation point then the ratio $a_1^2/a_0'^2$ of equation (70) is equal to $1-U'/U$. In other words, the term $va_1^2/a_0'^2$ is simply the local change of downwash angle at the blade due to the presence of the fuselage. Inserting into equation (70) the values appropriate to the case shown in Fig. 2 gives $\kappa/\kappa_0 = 1{\cdot}204$, i.e. the circulation increases by 20·4 per cent. Thus, comparing this value with that of Section 3.1. shows that the disturbance of the downwash by the fuselage is by far the most important interference to the lift of the blade.

This effect is not confined, of course, to the rotor downwash in hovering but to any component of velocity normal to the fuselage, e.g. in vertical flight or the component of forward velocity when the fuselage is tilted relative to the flight direction.

3.3. *Calculation of the Change of Lift on the Blade due to the Disturbance of the Downwash Flow Field by a Square Fuselage.*

We have seen in the previous section that the change of lift experienced by a blade as it passes over a fuselage can be calculated by finding the local change of inflow angle. This makes the calculation for the interference of a square fuselage fairly simple. We need a transformation which maps the exterior of a square onto the exterior of a circle since the flow about the latter can be written down easily. Such a transformation is given by Bickley in Ref. 8 where he uses the relation*

$$\frac{dz}{d\zeta}=\tfrac{1}{2}iC\ \mathrm{cosec}\ \alpha(1-2\zeta^{-2}\cos 2\alpha+\zeta^{-4})^{\frac{1}{2}} \tag{71}$$

---

*The numerical value of C given by Bickley, and quoted above, is consistent with the C of equation (71) and in what follows. Owing to the omission of a factor $\frac{1}{2}$ in Bickley's paper it is not consistent with the C of the transformation as first stated by him and from which the form of equation (71) has been derived.

to map the exterior of a rectangle in the z-plane conformally onto the exterior of a unit circle in the ζ-plane. For a square of side $2a$, $\alpha = \pi/4$, $k = 1/\sqrt{2}$ and $C = -ia/\sqrt{2}\ L$, where $L = E' - \frac{1}{2}K'$, (mod $1/\sqrt{2}$), i.e. $L = 0{\cdot}42361$.

Therefore

$$\frac{dz}{d\zeta} = \frac{a}{2L}(1+\zeta^{-4})^{\frac{1}{2}}. \tag{72}$$

Putting

$$dn\left(u, \frac{1}{\sqrt{2}}\right) = \tfrac{1}{2}(\zeta+\zeta^{-1}) \tag{73}$$

we get

$$\frac{dz}{du} = -\frac{ai}{2L}cn^2u \tag{74}$$

and integration gives

$$z = -\frac{ai}{L}\{E(u)-\tfrac{1}{2}u\}+D.$$

Bickley has further shown that $D = a$, giving finally

$$z = -\frac{ai}{L}\{E(u)-\tfrac{1}{2}u\}+a. \tag{75}$$

Now the complex potential of a unit circular cylinder in a uniform stream moving with velocity U in the negative ξ direction is

$$W = U(\zeta+\zeta^{-1})$$

giving

$$\frac{dW}{d\zeta} = U(1-\zeta^{-2}),$$

so that, using (72), the velocity components of an otherwise uniform stream flowing round a square will be

$$-u+iv = \frac{dW}{dz} = \frac{dW}{d\zeta}\cdot\frac{d\zeta}{dz} = \frac{2LU}{a}\cdot\frac{\zeta^2-1}{\sqrt{\zeta^4+1}}$$

and $\frac{dW}{dz} \to \frac{2L'U}{a}$ as $\zeta \to \infty$, i.e. the velocity at infinity is $\frac{2L'U}{a}$. Thus the ratio of disturbed velocity to the free stream velocity for the square is

$$\frac{\zeta^2-1}{\sqrt{\zeta^4+1}} = \frac{U'}{U}, \text{ say,}$$

and for the circle the corresponding ratio is $\frac{\zeta^2-1}{\zeta^2}$. Now, we are interested in the changes of downwash velocity for positions directly above the fuselage which correspond here to points along the positive real axis in both the $z-$ and ζ-planes. Hence we need a relationship between points on the real axis in the z-plane and corresponding points in the ζ-plane.

From equation (73) we obtain

$$sn\left(u, \frac{1}{\sqrt{2}}\right) = \frac{i}{\sqrt{2}}(\zeta - \zeta^{-1})$$

or

$$sc(iu) = \frac{1}{\sqrt{2}}(\zeta - \zeta^{-1}).$$

Therefore

$$u = isc^{-1}\left\{\frac{1}{\sqrt{2}}\left(\zeta - \frac{1}{\zeta}\right)\right\}$$

$$\equiv iu_1, \text{ say, for real values of } \zeta.$$

Therefore

$$u_1 = sc^{-1} f^2 \quad i.e.\ snu_1 = \frac{f}{\sqrt{1+f^2}} \tag{76}$$

where

$$f = \frac{1}{\sqrt{2}}\left(\zeta - \frac{1}{\zeta}\right). \tag{77}$$

Putting $\sin \varphi_1 = sn\, u_1$, we have, from (76)

$$\varphi_1 = \sin^{-1}\left(\frac{f}{\sqrt{1+f^2}}\right). \tag{78}$$

Now

$$z = -\frac{ai}{L'}\{E(u)-\tfrac{1}{2}u\}+a$$

and if $u = iu_1$

$$z = -\frac{ai}{L'}\{E(iu_1)-\tfrac{1}{2}iu_1\}+a$$

$$= \frac{a}{L'}\left\{\tfrac{1}{2}u_1-E(u_1)+\frac{sn\,u_1\,dn\,u_1}{cn\,u_1}\right\}$$

$$= \frac{a}{L'}\left\{\tfrac{1}{2}F(\varphi_1)-E(\varphi_1)+\frac{\sin\varphi_1\sqrt{1-\tfrac{1}{2}\sin^2\varphi_1}}{\cos\varphi_1}\right\}+a. \qquad (79)$$

Equations (77), (78) and (79) give us the required relationship. The velocity ratios U'/U at the same distances from a unit circle and unit square have been calculated and are shown in Fig. 12.

The numerical example of the previous sections gives $y = 1$ and for the square, from Fig. 12, we find $U'/U = 0{\cdot}63$. The change in the inflow angle is therefore $\left(1-\frac{U'}{U}\right)v = 1{\cdot}76$ deg, giving a change of incidence of 32 per cent, compared with 20·4 per cent for the circular fuselage. Thus, for this example, the square fuselage gives 60 per cent more blade interference than the circular one. When $y = 2$, i.e. when the blade is one diameter above the fuselage, the corresponding incidence, and therefore lift, increases are 13·1 per cent and 9 per cent for the square and circular fuselage respectively.

4. *The Mutual Interference between a Blade and a Lifting Wing in Forward Flight.*

Another important source of aerodynamic interference is that which will occur between a rotor blade and an auxiliary wing, as on a compound helicopter, or, what is the same thing, between a tailrotor and a tailfin. In what follows the term 'wing' will be used to mean either the wing of a compound helicopter or a tailfin since the analysis will be the same for both.

The mutual interference between the blade and wing can be considered as arising from three sources, namely

(a) the velocity interference from the bound vorticity or chordwise velocity distribution,
(b) the changing pressure field due to their relative motion, i.e. unsteady effects,
(c) the trailing velocity.

Sources (a) and (c) correspond to the well-known biplane interference but, unfortunately the established biplane theory is of little help since it has been developed mainly to calculate the steady drag and is not well suited to the calculation of lift variations.

The methods used to calculate the changes of blade lift will not be the same as those of the wing so that the interference effects to the blade and the wing will be considered separately.

4.1. *The 'end effect'.*

As in the previous sections the calculations will first be obtained from a two-dimensional analysis which will then be corrected for the 'end effect'. For the rotor blade this correction will be the same as in Section 2.5. For the wing or fin it will be assumed that the loading is uniform. This should be accurate enough for our purpose and also an analytical expression for the velocity distribution about a finite vortex of constant strength is known (e.g. Ref. 11, p. 128). Any other distribution, typical of a wing, would

be extremely difficult to integrate, if possible at all. By comparing the two-dimensional velocity distribution with that of a finite vortex we obtain a correction factor, k, for the wing given by

$$k = \frac{1}{2}\left\{\frac{\frac{\bar{y}}{s}+1}{\sqrt{\left(\frac{a}{s}\right)^2+\left(\frac{\bar{y}}{s}+1\right)^2}} - \frac{\frac{\bar{y}}{s}-1}{\sqrt{\left(\frac{a}{s}\right)^2+\left(\frac{\bar{y}}{s}-1\right)^2}}\right\} \tag{80}$$

where $\bar{y}$ is the spanwise distance from the centre of the wing
a is the distance of the blade axis from the wing
and s is the wing semi-span.

4.2. *Calculation of the Wing Lift.*

For this calculation the flow will be represented by a moving vortex, representing the blade, in the presence of a lifting flat plate, *see* Figs. 3 and 13a. The complex potential of this flow in the ζ-plane is

$$W = V_H\zeta e^{i\alpha_w} + V_H\frac{a_1^2}{\zeta}e^{-i\alpha_w} + i\kappa\log(\zeta+\zeta_0) + i\kappa\log\zeta - i\kappa\log\left(\zeta-\frac{a_1^2}{\zeta_0}\right) + i\kappa_w\log\zeta \tag{81}$$

where V_H is the helicopter speed, or its component along the chord if the wing or tailfin is swept back, and ζ_0 is the position of the blade vortex in the ζ-plane. It should be noted that the blade circulation is itself subject to interference. However, it should be sufficient here to assume the steady value, i.e. the value in the absence of interference. If required a second approximation can be made by considering the change of blade lift in the next Section.

As in Section 2.2., the force components are given by

$$X - iY = \tfrac{1}{2}i\rho\int_c\left(\frac{dW}{dz}\right)^2 dz - i\rho\int_c\frac{\partial\overline{W}}{\partial t}d\bar{z}.$$

The first integral represents the interference from source (a), mentioned in the previous section, and the second integral the inferference (b).

4.2.1. *Interference from bound vorticity.* The value of $\frac{1}{2}i\rho\int_c\left(\frac{dW}{dz}\right)^2 dz$ has been calculated by Neumark[9], who uses exactly the same mathematical model to investigate the effect of a rotating flap on the characteristics of an aerofoil. The complete solution is rather long, however, and takes into account not only the change of circulation induced by the vortex (representing the rotating flap in Neumark's case) but also the change of pressure distribution over the aerofoil due to the non-uniformity of the external flow. The terms corresponding to the latter are small for the cases in which we are interested and a much simpler expression can be obtained by considering the effect of the change of circulation only. This can be obtained, of course, by retaining the appropriate terms of Neumark's result but it can be derived quite simply by using Milne-Thomson's theorem, equation (62), of Section 3.2. For in this case $f(\zeta)$ is simply $V\zeta e^{i\alpha_w} + i\kappa\log(\zeta-\zeta_0)$, so that putting $\zeta_0 = a_0e^{i\chi_0}$, and since $\zeta = -a_1$ is a stagnation point, we easily find that the change of circulation $2\pi\Delta\kappa_w$ is given by

$$\kappa_w + \Delta\kappa_w = 2a_1 V_H \sin\alpha_w \pm \frac{2\kappa k'(k'+\cos\chi_0)}{1+2k'\cos\chi_0+k'^2} \tag{82}$$

where $2\pi\kappa_w$ is the steady wing circulation, $k' = a_1/a_0$, and the negative and positive signs refer to the advancing and retreating blades respectively.

Since $4\pi\kappa = V'cC_L$, where V' is the relative airspeed of the blade section, that is $V' = \Omega R(x+\mu \sin \psi)$, we can write

$$\Delta\kappa_w = \mp\frac{V'cC_Lk'(k'+\cos\chi_0)}{2\pi(1+2k'\cos\chi_0+k'^2)} \tag{83}$$

and the (two-dimensional) change of lift is given by

$$\begin{aligned}\Delta L' &= 2\pi\rho\Delta\kappa_w V_H \\ &= \mp\frac{\rho V_H V'cC_Lk'(k'+\cos\chi_0)}{1+2k'\cos\chi_0+k'^2}.\end{aligned} \tag{84}$$

Now the change of lift on a finite wing will be smaller than this due to its own trailing vortex system. To correct for this we assume that the ratio of the increment of lift on a finite wing to that of an infinite wing is the same as the ratio of their respective lift slopes for which a simple expression exists for elliptic loading (Ref. 11, p. 145). Thus, if the increment of lift for the finite wing of aspect ratio A is ΔL we assume that

$$\Delta L = \frac{A}{A+2}\Delta L'. \tag{85}$$

4.2.2. *Interference due to unsteady flow.* Since the first two terms of equation (81) are independent time, and if the time derivatives of κ and κ_w are assumed to be small, the contribution of $\frac{\partial \overline{W}}{\partial t}$ to $X - iY$ is identical to that of Section 2.3., that is, in terms of the blade circulation

$$\left.\begin{aligned}X &= 0 \\ Y &= \frac{4\pi\rho\kappa Vk'^2(\cos 2\chi_0 - k'^2)}{1-2k'^2\cos 2\chi_0+k'^4}\end{aligned}\right\}. \tag{24}$$

In terms of the blade chord and lift coefficient we can also write

$$Y = \frac{\rho V V'cC_Lk'^2(\cos 2\chi_0 - k'^2)}{1-2k'^2\cos 2\chi_0+k'^4} \tag{24a}$$

where V is the speed of the blade relative to the wing, that is $V = \Omega r$. No distinction need be made in this case between the advancing and retreating blade because relative to the chosen axes both the signs of the vortex strength and the velocity, $V = \partial z_0/\partial t$, change together.

4.2.3. *Interference due to trailing vorticity of blade.* It is unlikely that the trailing vortex system from the rotor will produce significant timewise variations of wing lift. There might be a slight local increase of induced velocity near the blade but we will assume that at any given point under the rotor the induced velocity is constant. The steady induced velocity will, of course, take part in determining the steady wing lift. No simple theory exists for the estimation of the induced velocity below a rotor but the wind-tunnel tests of Heyson[10], provide an adequate set of data from which an accurate estimation can be made.

4.3. *The Calculation of Blade Lift.*

In all the work so far we have been able to represent the flow about a rotor blade by a vortex since the blade has always been at least its own chord's distance from the surface it has been affecting. When we consider the interference of a lifting wing on the blade, however, we note that the wing chord is usually much greater than that of the blade and that the separation between the wing and a blade is often much less than the wing chord, e.g. the tailrotor blades of the Westland 'Wessex' come within a quarter of the tailfin chord of the tailfin. Therefore, as far as the blade is concerned, we may not always be justified in approximating to the wing flow by a vortex and a more suitable representation, such as in Section 4.3.2. below, may have to be found.

4.3.1. *Interference due to chordwise flow about wing.* In order to calculate the chordwise flow about the wing we can, in this case, assume the wing flow to be represented by the flow about a lifting flat plate. Also, since the chord of the blade is much smaller than that of the wing, the blade can be treated as if it were a line, in which case it is necessary only to calculate the local change of incidence at the line instead of having to consider the distribution along the blade chord. The circulation about the wing should be taken as the one appropriate to its aspect ratio and incidence and which, therefore, will not satisfy the Kutta-Joukowski trailing edge condition. However, as we are also going to consider the effect of the trailing vortices from the wing, the trailing edge condition will, in effect, be satisfied and the steady flow about the wing properly accounted for.

The change of incidence at the blade is easily calculated. The complex potential of the flow about the wing's transforming circle in the ζ-plane is

$$W = V_H \zeta e^{i\alpha_w} + V_H \frac{a_1^2}{\zeta} e^{-i\alpha_w} + i\kappa_w \log \zeta$$

where we have omitted the image vortices of the blade since they will only affect the flow very close to the wing surface.

The velocity components u and v in the z-plane are given by

$$\begin{aligned} -u+iv &= \frac{dW}{dz} = \frac{dW}{d\zeta}\frac{d\zeta}{dz} \\ &= V_H e^{i\alpha_w} + \frac{2ia_1^2 V_H \sin\alpha_w}{\zeta^2 - a_1^2} + \frac{i\kappa_w \zeta}{\zeta^2 - a_1^2} \\ &= V_H e^{i\alpha_w} - u' + iv', \text{ say,} \end{aligned}$$

where u' and v' represent the disturbance due to the wing or fin and are relative to the main stream direction. The change of incidence at the blade is approximately $v'/V' = \Delta\alpha_1$, say.

Putting $\zeta_0 = a_0 e^{i\chi_0}$ for the co-ordinates of the centre of the blade, and $k' = a_1/a_0$, gives

$$\Delta\alpha_1 = \frac{k'\dfrac{V_H}{V'}}{1 - 2k'^2\cos 2\chi_0 + k'^4}\left\{2k'\sin\alpha_w\left(\cos 2\chi_0 - k'^2\right) + \frac{C_{Lw}}{\pi}(1-k'^2)\cos\chi_0\right\} \tag{86}$$

where C_{Lw} is the lift coefficient of the wing.

Then, if L_0 is the steady lift of the blade element, and if α is the local blade incidence, the change in lift from the above contribution will be $\dfrac{\Delta\alpha_1}{\alpha} L_0$. The effective change of tailrotor shaft angle is the same as that given by equation (86) but with $\dfrac{V_H}{V'}$ replaced by unity.

4.3.2. *Interference due to unsteady flow.* When the rotor blade is more than a wing chord distance from the wing the unsteady lift change can be found from equation (24a) of Section 4.2.2., but with $V'cC_L$ being replaced by $V_H c_w C_{Lw}$ and a negative sign in front of the expression since the wing vortex moves in the negative sense relative to the blade.

For cases where the blade is very close to the wing or fin the simple vortex representation of the wing flow is no longer valid and a better representation must be found.

The flow about a flat-plate aerofoil, however, is too complicated to be able to find the timewise pressure variations easily and we must now make some sort of compromise between a lifting flat plate and a vortex. Now we know from aerofoil theory that a thin aerofoil can be represented by a vortex sheet and, as we have results already for the effect of one moving vortex, it would seem that a convenient second approximation to an aerofoil might be tried in which the aerofoil is represented by two vortices instead of one. Let us place one vortex, of strength κ_1, at the $\frac{1}{4}$ chord point and the other, of strength κ_2, at the $\frac{3}{4}$ chord point and choose these strengths, as in aerofoil theory, such that their combined circulation is equal to the circulation of the aerofoil they represent. We also choose the boundary condition at the $\frac{1}{2}$ chord point to be satisfied. The latter choice above is somewhat arbitrary but the results seem to be quite satisfactory as shown below. If κ_w is the local wing vortex strength, the strengths of the two vortices at the $\frac{1}{4}$ and $\frac{3}{4}$ chord points are easily found to be $\frac{1}{2}\left(\kappa_w+\frac{4}{c_w}V_H \sin\alpha\right)$ and $\frac{1}{2}\left(\kappa_w-\frac{4}{c_w}V_H \sin\alpha\right)$ respectively. Calculations have been made of the steady pressure coefficient for the flat plate, single vortex and double vortex at two positions close to the aerofoil which is at 5·7 deg incidence. The results are given in the table below.

Position relative to aerofoil	Flat plate	Single vortex	Double vortex
5/24c above centre	−0·184	−0·538	−0·209i
$\frac{1}{8}$c above and $\frac{1}{4}$c behind L.E.	−0·438	−0·125	−0·360

We now find the normal velocity, w'', on the longitudinal axis from the trailing vortex system of the wing. This calculation will differ from Glauert's calculation of the downwash angle, $\varepsilon = \frac{w}{V}$, since he included the downwash from the bound vortex, representing the chordwise flow about the aerofoil, whereas, in our case, this has already been taken into account.

The normal induced velocity on the $\bar{x}$ axis at a point l behind the wing from two trailing vortices, distance s' apart, is

$$w'' = \frac{\kappa}{s'}\left\{1+\frac{l}{\sqrt{l^2+s'^2}}\right\}$$

so that for elliptic loading when $\kappa = \frac{2w_0}{\pi}\sqrt{s^2-\eta^2}$,

$$w'' = \frac{2w_0}{\pi}\int_0^s \left\{\frac{1}{\sqrt{s^2-\eta^2}}+\frac{l}{\sqrt{(l^2+\eta^2)(s^2-\eta^2)}}\right\} d\eta .$$

Putting $\eta = s\cos\theta$ and $l^2 = \dfrac{1-k^2}{k^2}s^2$ gives

$$w'' = \frac{2w_0}{\pi}\int_0^{\pi/2}\left\{1 \pm \sqrt{\frac{1-k^2}{1-k^2\sin^2\theta}}\right\}d\theta$$

$$= w_0\left\{1 \pm \frac{2K}{\pi}\sqrt{1-k^2}\right\} \tag{88}$$

where K is the complete elliptic integral of the first kind, of modulus k, and the positive and negative signs refer to points behind and in front of the wing respectively. We note that at the wing $k = 1$ and equation (88) reverts to equation (87), as it should.

We now assume that the normal induced velocity distribution in the lateral plane through the wing, given by equation (87), applies to all lateral planes and that the magnitude of the velocity, at a given point, varies in the same way as the velocity along the longitudinal axis. This means that we replace the w_0 of equation (87) by the w'' of equation (88) to obtain, for a general position,

$$w = w_0\left(1 - \frac{\sinh\mu\cosh\mu}{\cosh^2\mu - \sin^2\lambda}\right)\left(1 \pm \frac{2K}{\pi}\sqrt{1-k^2}\right)$$

where, in our notation,

$$w_0 = \frac{V_H C_{L_w}}{\pi A} \tag{89}$$

and A is the aspect ratio of the wing.

Equations (87) and (88) have been plotted for ranges of $\bar{y}/s$, $\bar{z}/s$ and l/s and are shown in Figs. 15 and 16. Thus to obtain w we calculate w_0 from equation (90) and multiply successively by the factors $\dfrac{w'}{w_0}$ and $\dfrac{w''}{w_0}$ obtained from Figs. 15 and 16. This method of approximation has been tested by applying it also to the calculation of the flow about a uniformly loaded wing for which it is comparatively easy to calculate the exact velocity. The approximation was found to be good.

4.4. *Numerical Examples of Rotor/Wing Interference.*

4.4.1. *Interference to the lift of the wing of the Westland 'Rotodyne'.* The variation of lift near the tip of the wing of the Westland 'Rotodyne Y' has been calculated using the theory of Section 4.1. The flight conditions were taken from the tests of Ref. 12 for a case in which the tip speed ratio was 0·35. The radial position on the blade chosen for calculation was $\dfrac{r}{R} = 0{\cdot}5$ and as it was well away from the rotor tip it was thought necessary to apply the end correction of Section 2.5. The percentage variation of lift with azimuth position of the blade is shown in Fig. 17a and can be seen that it is small. The calculations showed that the contributions from the unsteady pressures and the interference from the bound vortex flow are of about the same order in this case.

4.4.2. *Interference to the lift of the blade of the Westland 'Rotodyne'.* Fig. 17b shows the percentage variation of lift at the radial position, $\dfrac{r}{R} = 0{\cdot}5$, of the advancing blade. It will be seen that the variation is large and arises from the fact that the steady state incidence is only about 1 degree whereas the bound vortex flow, corrected by the factor of equation (80) and Fig. 14, causes an incidence change of between $+0{\cdot}4$ degrees and $-0{\cdot}4$ degrees. The unsteady lift variation is negligible. Fig. 14 shows that beyond the

wing-tips the interference of the wing falls off very rapidly so that, for the 'Rotodyne', the interference of the wing on the rotor blade does not extend much beyond $\frac{r}{R} = 0{\cdot}5$. Thus, although the percentage interference is high at $\frac{r}{R} = 0{\cdot}5$ the interference to the whole blade is quite small.

4.4.3. *Interference to the lift of the tailfin of the Westland 'Wessex'.* The change of lift on a section of the tailfin of the Westland 'Wessex' has been calculated the results being shown in Fig. 18a. The blade radial position has been taken at $\frac{r}{R} = 0{\cdot}75$ and it has been assumed that the local lift coefficient of the advancing tailrotor blade is 0·2 and that the forward speed of the helicopter is 170 ft/sec. It can be seen that by far the most important effect is the unsteady pressure component and this is to be expected as the rotor is only about 1·3 feet away from the fin whose chord is about 4 feet.

Now since the unsteady forces are independent of the forward speed of the helicopter this suggests that the greatest interference effects will occur in the hovering condition when the lift coefficient of the advancing blade will be at its highest. No detailed blade loading analysis has been made but it has been assumed that in hovering flight, and in free air, the blade lift coefficient is 0·41. This means that the unsteady forces would be just over twice as large as those shown in Fig. 18a. These forces have been calculated over the whole blade, with the appropriate end correction applied, and the result is shown in Fig. 18b. The total maximum force on the fin is 102 lb and its variation with azimuth angle is the same as in the broken curve of Fig. 18a. The curve is shown for a range of azimuth of 90 deg which means that, since the 'Wessex' has four blades, the pattern repeats itself immediately. The mean value of this force is found to be 60 lb and is in a direction opposite to that of the tailrotor thrust. Assuming, from the known power in hovering, that the tailrotor thrust is 870 lb, the interference force represents a loss of tailrotor effectiveness of about 7 per cent. However, the above calculation is conservative as no account has been taken of the effect of the fin on the tailrotor induced-velocity field which in hovering would be very large. The 'Wessex' fin is upstream of the tailrotor and it is probable that in the wake behind the fin the air velocity is practically zero. Thus, since the induced velocity at the rotor tip is about 85 ft/sec, the blade would experience an increase of incidence of about $7\frac{1}{2}$ deg as it came into the lee of the fin. Even in potential flow the increase of incidence would be about $3\frac{1}{2}$ deg, as can be seen from Fig. 12 for the case $y = 0{\cdot}65$. The lift of the blade interfering with the fin would probably be doubled at least (if it had not already stalled), producing double the force calculated above and which would now represent a loss of about 14 per cent.

In addition to the above there is the steady force on the fin from the tailrotor downwash. This is difficult to estimate accurately as it cannot be assumed that the force is simply $C_D \frac{1}{2}\rho v_i^2 S$ (where v_i is the local downwash velocity and C_D a flat-plate drag coefficient) as the static pressure is varying rapidly in the neighbourhood also. Nevertheless the force is almost certain to be in the adverse sense and may well increase the total loss to about 20 per cent.

It appears, then, that tailrotor/tailfin interference is one of the most important cases of interference encountered on the helicopter and, from the above calculations, might be expected to become serious when the chord of the tailfin becomes greater than about half the tailrotor radius.

4.4.4. *Interference to the lift of the tailrotor of the Westland 'Wessex'.* In straight unyawed flight the only interference to the tailrotor expected from the tailfin would be the dynamic pressure forces. Calculations show that these forces are small and are at most about 1 per cent of the blade lift. Interference effects become important when the aircraft yaws as the tailfin straightens the airflow near the tailrotor so that the apparent yaw angle of the tailrotor is reduced and hence also its effectiveness as a fin. An example of this is shown in Fig. 18c where the apparent change of incidence of the no-feathering axis of the rotor, as felt by a blade near the fin, is much less than the actual change. The figures given in Fig. 18c suggest that the fin-effectiveness of the tail rotor is reduced by about 17 per cent. At low speeds and in hovering, when streamline flow about the fin has not become established, this interference effect will not be apparent but the 'shielding' effect from the downwash, mentioned in Section 4.4.3. above, will be important.

5. *Comparison of Theory with Experimental Results.*

5.1. *Comparison with NASA Cylinder Tests.*

Ref. 1 describes a series of tests in which pressures were measured on a circular cylinder under a hovering rotor. Measurements were made for four different rotor heights at seven pressure orifices equally spaced from the top to the bottom of the cylinder around one half of its circumference. Variations of pressure with radial distance from the axis of the rotor were obtained by progressively moving the cylinder from one side of the rotor to the other. However, the pressure orifices were not in the middle of the cylinder but close to one end, which meant that the cylinder rarely spanned a rotor radius when the orifices were in the slipstream and also, for a given radial position of the orifices, the amount of cylinder in the slipstream differed according to which side of the rotor the orifices were placed. Aerodynamically speaking, part of the image vortices were usually missing and, due to the asymmetry mentioned above, the pressure measurements made on one side of the rotor should have been different from those made at the corresponding radius on the other side. Figs. 19 and 20 show that this was the case and the lower set of points, indicated by the empty circles, correspond, as would be expected, to the shorter length of cylinder.

It is possible to calculate curves of pressure against radius taking into account the appropriate length of cylinder for each point, but as this would be very tedious it was decided to compute two curves, the one corresponding to the cylinder completely spanning the rotor radius and the other corresponding to the complete absence of the cylinder. The experimental points should lie between these curves. The C_L-distribution used in the theory was obtained from the usual strip theory with the blade lift-slope adjusted to give the same disc loading as quoted in the tests. Experimental points were omitted whose values were clearly affected by the trailing vortex of the blade. Figs. 19 and 20 show that, apart from obvious scatter, the theory over-estimates the pressures slightly but that the agreement generally is quite good.

5.2. *Comparison with R.A.E. Cylinder Tests.*

Tests have been made at R.A.E. (Bedford) similar to those discussed in the previous Section. The main difference was that the cylinder had an adjustable extension so that for every radial orifice position the length of cylinder in the slipstream could be adjusted to span most of the rotor radius. In this way the source of errors, mentioned in the previous Section, were largely avoided. A detailed description of the apparatus and test procedure is given in Appendix B.

Tests were made with the rotor hub placed at one chord and two chord height above the cylinder. The comparison between theory and experiment for the first case has already been given in Fig. 10. The comparison for the second case (two chord height) is shown in Fig. 21. Agreement is seen to be good generally. Again, measurements obviously affected by the blade trailing vortex, at about the position $\frac{r}{R} = 0{\cdot}9$, have been omitted.

Fig. 22 shows the theoretical and measured variation of pressure with blade azimuth angle at the top of the cylinder at the radial positions $\frac{r}{R} = 0{\cdot}785$ and $\frac{r}{R} = 0{\cdot}585$. Agreement can be seen to be very good.

5.3. *Comparison with NASA Flat-plate Tests.*

Fig. 23 shows some of the measurements, from Ref. 2, of the variation of pressures at the centreline of a flat panel as a rotor blade passes over it. The measurements were made at two different disc loadings and the theory indicates that, owing to the difference in coning angle for the two cases, there should be a considerable difference in pressure variation. However, only one experimental curve is given in Ref. 2 for each rotor height and these are compared with the theoretical curves for the higher disc loading. Agreement is quite good, except near the blade tip, but since it is not known how the curves were derived from the experimental points, which the theory suggests should have been in two distinct sets, the agreement may well be fortuitous.

5.4. *Comparison of Estimated Blade Lift with R.A.E. Measurements.*

Fig. 24 shows the theoretical differential pressure distribution for a flat-plate for steady conditions, and when passing over a circular fuselage, for the conditions stated. Experimental points for the blade NACA 0012 aerofoil are shown for comparison. The figure is interesting mainly because of the similarity in distribution between the flat plate, which is comparatively easy to calculate, and the NACA 0012 aerofoil. The increase in lift, for the case quoted, is not very obvious from the figure but has been calculated to be 15·2 per cent due to the increase in circulation (*see* Section 3.2.). (This figure is smaller than that calculated in Section 3.2. as here coning angle has been taken into account.) The measured increase in lift was found to be 15·5 per cent so that agreement between theory and experiment is good.

Fig. 25 shows the variation of lift with blade azimuth angle.

6. *Acknowledgment.*

The authors wish to thank Dr. G. M. Roper of Aero Department for her kind advice and interest in this work, and in particular for suggesting the transformation of Section 2.4. as being the most suitable for our purpose and leading to an exact value of the modulus k.

LIST OF SYMBOLS

a	Radius of circular fuselage
a_1	Radius of transforming circle in ζ-plane
a', a''	Radial co-ordinates of image vortices in ζ-plane
a_0	Radial co-ordinates of blade vortex in ζ-plane
a	Semi-length of side of square
A	Constant determing scale and orientation in transformation, equation (27)
b	Co-ordinate of vortex along imaginary axis in τ-plane
c	Blade chord
C_w	Wing chord
C_{L_w}	Lift coefficient of wing element
C_L	Lift coefficient of blade
C	Factor used in determining scale of transformation, equation (71)
$cn(u,k)$	An elliptic function
$dn(u,k)$	An elliptic function
$E(u,k)$	Incomplete elliptic integral of the second kind
E, E'	Complete elliptic integrals of the second kind
f	Factor used in determining 'end effect', Section 2.5.
h	Height of blade above fuselage, *see* Fig. 8
I_1, I_2, I_3	Integrals defined by equations (47), (48) and (49)
k	a/a_0
k	Factor used in determing 'end effect', Section 4.1.
k, k'	Moduli of elliptic functions
k'	a_1/a_0
K, K'	Complete elliptic integrals of the first kind
l	Co-ordinate of point on fuselage, *see* Fig. 8
L	$E-\frac{1}{2}K$ (mod $1/\sqrt{2}$)
L_0	Steady lift of blade element
p	Air pressure
p_0	Atmospheric pressure
p'_0	Undisturbed pressure at point on circular cylinder
q	Air velocity
r	Radial distance of blade element from hub
R	Radius of blade

LIST OF SYMBOLS—(*contd.*)

s	Semi-span of wing
u	Component of velocity along x-axis
u'	Component of velocity along x-axis due to interference of wing
u, u_1	Variables of elliptic functions
U	Local downwash velocity
v	Component of velocity along y-axis
v'	Component of velocity along y-axis due to interference of wing
V	Velocity of a blade element
V_H	Velocity of helicopter or its chordwise component over a swept wing or fin
V_τ	Velocity of vortex in τ-plane
w_0	Induced velocity at elliptically loaded wing
W	$\varphi + i\psi$, complex potential
w, w', w''	Normal components of induced velocity near wing
x	r/R
x, y	Co-ordinates axes of physical plane
$\bar{x}, \bar{y}, \bar{z}$	Co-ordinates of a point from a lifting wing
X, Y	Force components along x, y axes
y_0	Distance of blade vortex above square fuselage
y	$= y_0/a$
α	Incidence of blade element
$\Delta\alpha_1$	Change of incidence at blade element due to bound vorticity of wing
α	k/b, *see* equation (46)
α	Parameter used in determining scale of transformation, equation (71)
β	Angular co-ordinate used in determining end effect, *see* Fig. 8
γ	h/R
ε	l/R
ε	w/V, downwash angle behind wing
ζ	$\xi + i\eta$, complex co-ordinate in transformed plane
ξ, η	Co-ordinates in transformed plane
θ	Angular co-ordinate of a point on circular fuselage
θ_0	Angular co-ordinate of blade vortex
ϑ_0	Collective pitch angle of blade
κ	Vortex strength

κ_0	Steady vortex strength of blade
κ_w	Steady vortex strength about wing
λ	$(1-k)/(1+k)$ modulus transformation of elliptic functions
v	U/V
$\Pi(K,-\alpha^2,k)$	Complete elliptic integral of the third kind
ρ	Air density
ρ,σ	Co-ordinates in τ-plane, *see* Fig. 4
φ	Velocity potential
χ	Angular co-ordinate in ζ-plane
ψ	Stream function
Ω	Angular velocity of rotor

REFERENCES

No.	*Author(s)*	*Title, etc.*
1	John W. McKee	Experimental investigation of the pressure fluctuations on a flat plate and a cylinder in the slipstream of a hovering rotor. NASA Technical Note D–112, September, 1959.
2	Robert A. Makofski and George F. Menkick ..	Investigation of vertical drag and periodic airloads acting on flat panels in a rotor slipstream. NASA T.N. 3900, December, 1956.
3	L. M. Milne-Thomson ..	*Theoretical aerodynamics.* Macmillan & Co. Ltd. 1948.
4	Harry H. Heyson	An evaluation of linearized vortex theory as applied to single and multiple rotors hovering in and out of ground effect. NASA Technical Note D–43, September, 1959.
5	L. M. Milne-Thomson ..	*Theoretical hydrodynamics* 2nd Edn. Macmillan & Co. Ltd. 1949.
6	H. Bateman	*Partial differential equations of mathematical physics.* Dover Publications.
7	Paul F. Byrd and Morris D. Friedman	*Handbook of Elliptic Integrals for Engineers and Physicists.* Springer Verlag, Berlin.
8	W. G. Bickley	*Proc. London Math. Soc.* 1934, Vol. 37(II).
9	S. Neumark	Two-dimensional theory of an aerofoil with rotating flap. R.A.E. Report No. Aero 2641, July, 1960. ARC 22540.
10	Harry H. Heyson	Induced velocities near a lifting rotor with non-uniform disc loading. NACA Report No. 1319.
11	H. Glauert	*The elements of aerofoil and airscrew theory.* Cambridge University Press.
12	—	Further rotor and fuselage trim characteristics of the Rotodyne aircraft in autogyro flight. Flight Analysis Report No. Y.8. Fairey Aviation Ltd.

APPENDIX A

Relationships between Co-ordination in the ζ and z Planes

In Sections 2.3., 4.1. and 4.2. we need the relationships which express the variables k' and χ in the ζ-plane. The transformation connecting ζ and z is

$$z = \zeta + \frac{a_1^2}{\zeta}$$

giving

$$\zeta = \frac{1}{2}\left(z + \sqrt{z^2 - 4a_1^2}\right)$$

where we have chosen the positive sign in front of the radical since we want the transformation which maps the outside of the circle in the ζ-plane onto the whole z-plane. Putting $\zeta = a_0 e^{i\chi}$ and $k' = a_1/a_0$ we find after some algebra

$$k' + \frac{1}{k'} = \sqrt{\frac{x^2 + y^2 + 4a_1^2 + \sqrt{W}}{2a_1^2}}$$

$$k' - \frac{1}{k'} = -\sqrt{\frac{x^2 + y^2 - 4a_1^2 + \sqrt{W}}{2a_1^2}}$$

$$\sin\chi = \frac{y}{a_1}\sqrt{\frac{4a_1^2 - x^2 - y^2 + \sqrt{W}}{8y^2}}$$

$$\cos\chi = \frac{x}{a_1}\sqrt{\frac{x^2 + y^2 + 4a_1^2 - \sqrt{W}}{8x^2}}$$

where, as defined in Ref. 8,

$$W = (x^2 + y^2 + 4a_1^2)^2 - 16a_1^2x^2$$

$$= (x^2 + y^2 - 4a_1^2)^2 + 16a_1^2y^2 .$$

APPENDIX B

Pressure Measurements on a Cylinder in the Downwash of a Hovering Rotor

1. *Description of Test Equipment.*

Pressure measurements were made on the upper surface of a one foot diameter cylinder placed, with its longitudinal axis horizontal, in the downwash of a hovering 12 ft diameter helicopter rotor. The test rig is shown in Fig. 26. The aerofoil section of the blades was NACA 0012 and the chord constant at 6 inches; there was a flapping hinge at 3·1 per cent and a drag-hinge at 6·6 per cent of the blade radius. The tests were carried out in a large hangar where the floor was about one and quarter rotor diameters below the plane of the disk and the roof a slightly greater distance above it.

A light-weight steel framework supported the cylinder, which had a nominal length of 10 ft. As shown in Fig. 27 only two sets of pressure plotting holes were used so that, to obtain the distribution along the axis of the cylinder, the whole support frame and cylinder were shifted radially outwards in a series of small movements until the survey was complete. To avoid possible end-effects due to the finite length of the cylinder the outer end was never less than 4·75 ft beyond the outer edge of the rotor disk. At the inner edge of the disk the minimum distance between a pressure measuring point and the cylinder end was 1·56 ft; this occurred when the cylinder was touching the casing of the electric-motor used to drive the rotor. When the framework was moved outwards a sliding portion of the cylinder was used to maintain an adequate length between this pressure point and the inner end.

Inductive type electrical transducers were used to measure the pressures (*see* Figs. 28 and 29). On the rotor blade these were recorded at the 75 per cent radius position only; each transducer gave a net value between the upper and lower surfaces of the blade. On the cylinder the difference between the local surface pressure and that of the air well away from the rotor was recorded.

2. *Test Conditions.*

All tests were made with the collective pitch of the blades set at 10 deg and the rotor running at 570 r.p.m. (tip speed = 357 ft/sec). Records were taken with the top surface of the cylinder 6 inches below the centreline of the blade flapping hinge and with this distance increased to 12 inches; i.e. 1 and 2 blade chords or $\frac{1}{2}$ and 1 cylinder diameters below the disk respectively. The cylinder was kept parallel to the floor of the hangar but the rotor blades, when rotating, coned upwards about $1\frac{3}{4}$ deg.

The innermost pressure point on the cylinder axis was situated beneath the 38 per cent radius position. The cylinder was then moved outwards in steps of 0·3 ft (5 per cent R) until this pressure point was beneath the 98·5 per cent radius position.

3. *Results.*

Galvanometer deflections due to signals from the transducers were recorded on photographic paper; typical traces are shown in Fig. 30. The relative magnitude of the deflections shown cannot be compared directly because of differing transducer sensitivities and signal amplifications. After resolving these differences by applying the appropriate calibration factors the deflections were reduced to pressure values. The results for the spanwise distribution of pressure increment due to the passage of the blade over the cylinder are shown in Figs. 10 and 21. The variation of this increment at a particular station as the blade approached and then receded away from the cylinder is shown in Fig. 22. Fig. 24 shows the net chordwise pressure distribution on the rotor blade, at 75 per cent radius; a small temporary increase in lift was measured as the blade passed over the cylinder.

This increase is shown on the records (Fig. 30) as a peak in the galvanometer traces occurring once per revolution because only one blade out of the three contained transducers. The corresponding peaks in pressure on the cylinder obviously are shown three times per revolution of the rotor (i.e. at 28·5 times

per sec). From previous tests on the blade installation it had been found that the overall frequency response of the pressure plotting system was linear up to at least 30 cps. By interpolation it was estimated that linearity would be achieved up to 55 c/s for the installation on the cylinder, which had shorter pipe lengths. Except in the region beneath the blade tip, these calibration tests, the orderly nature of the records, and the lack of any discernible lag between the pressure rises on the blade and those on the cylinder indicate that the results represent an accurate record of the pressure changes that occurred. The effect on the galvanometer deflections when the measuring station was placed beneath the rotor tip is shown by the lower records in Fig. 30. It can be seen that there are large negative values of pressure just after the positive pressure peak. Traces taken with the cylinder 12 inches below the rotor showed similar negative values occurring just before the blade reached the cylinder. These large disturbances are believed to be due to the pressure and flow variations caused by the tip vortices of the blade above the cylinder and of the preceding blade. This effect, which was also observed in the NASA tests, was even more marked at other radial positions close to the 93·5 per cent station shown in Fig. 30. It was felt that the response of the measuring system to these large and rapid variations would adversely affect the accuracy of the positive pressure peaks under investigation. Any records taken near the blade tip which showed signs of such degradation have been ignored in the presentation of the results in this Report.

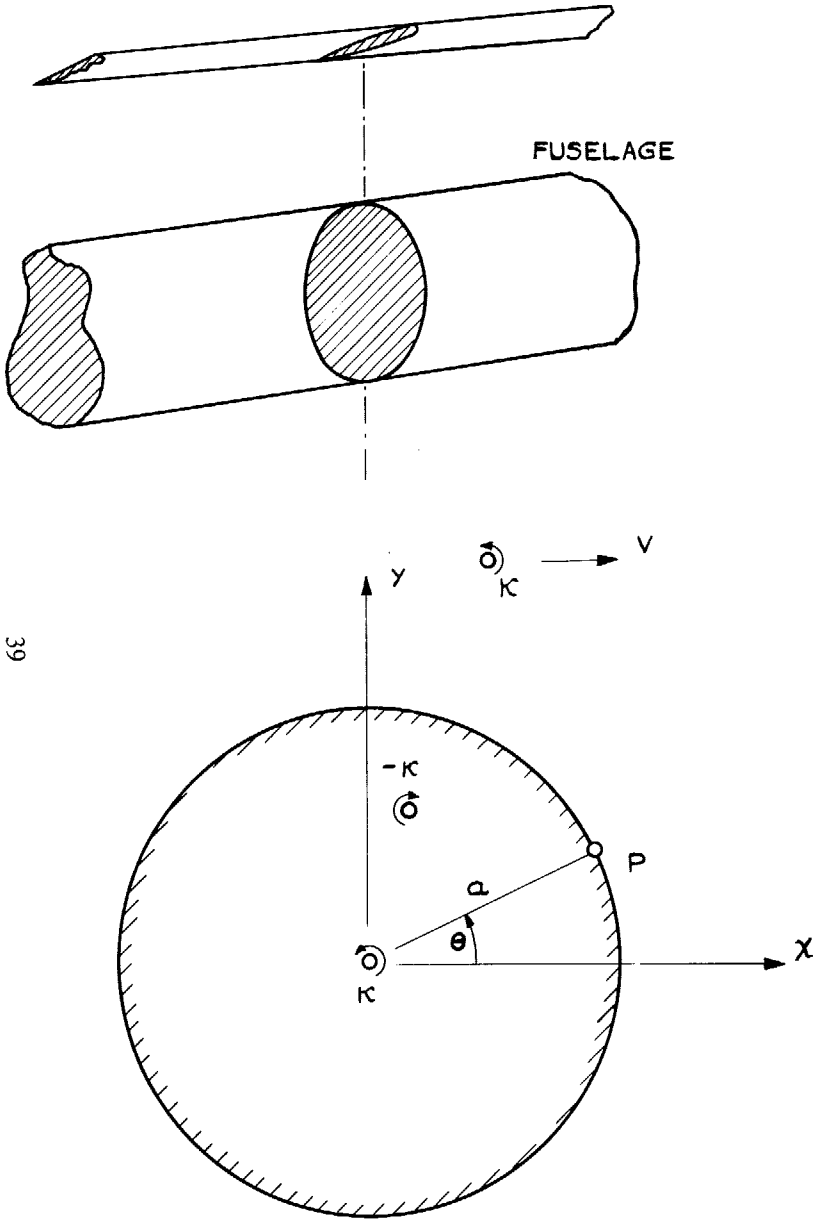

FIG. 1. Image system for vortex in presence of circular cylinder.

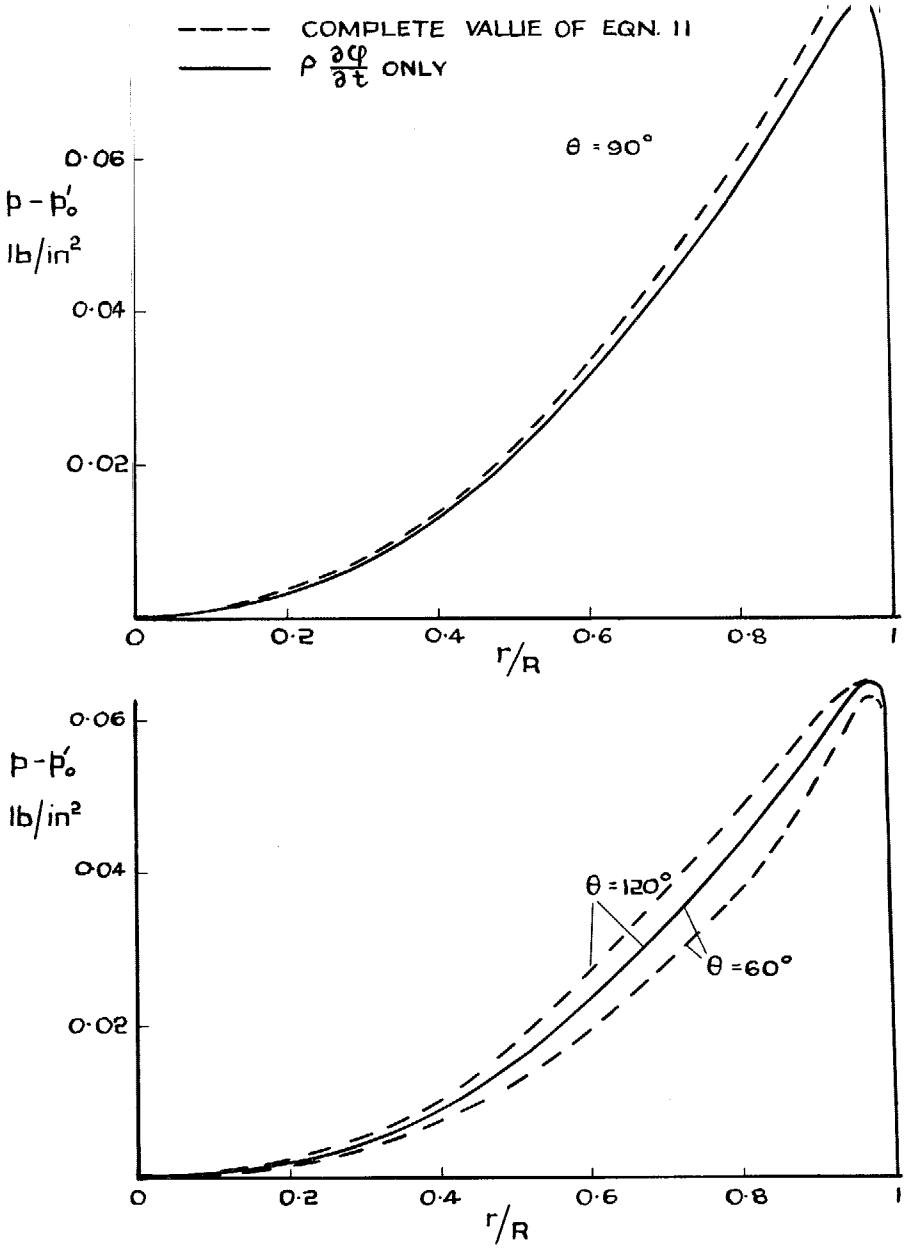

FIG. 2. Calculated value of pressure on a circular fuselage. (No end connection) $\theta_0 = 90$ deg, $C = 0{\cdot}5$ ft, $\alpha = 0{\cdot}5$ ft, $\alpha_0 = 1$ ft, $\Omega R = 357$ ft/sec, $\vartheta = 11$ deg, Lift slope = 5·5.

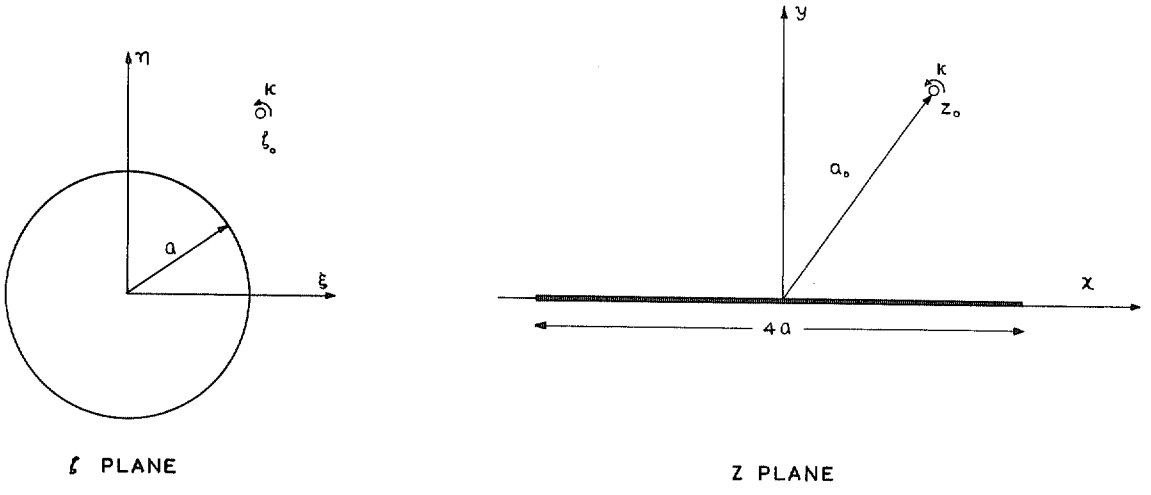

FIG. 3. Transformation of circle into flat-plate aerofoil.

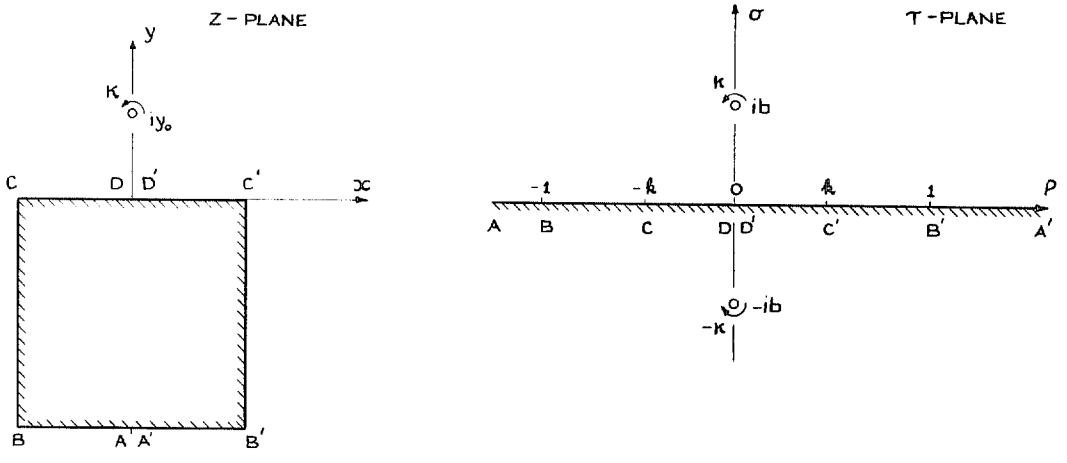

FIG. 4. Mapping of a vortex in the τ-plane onto the outside of a square.

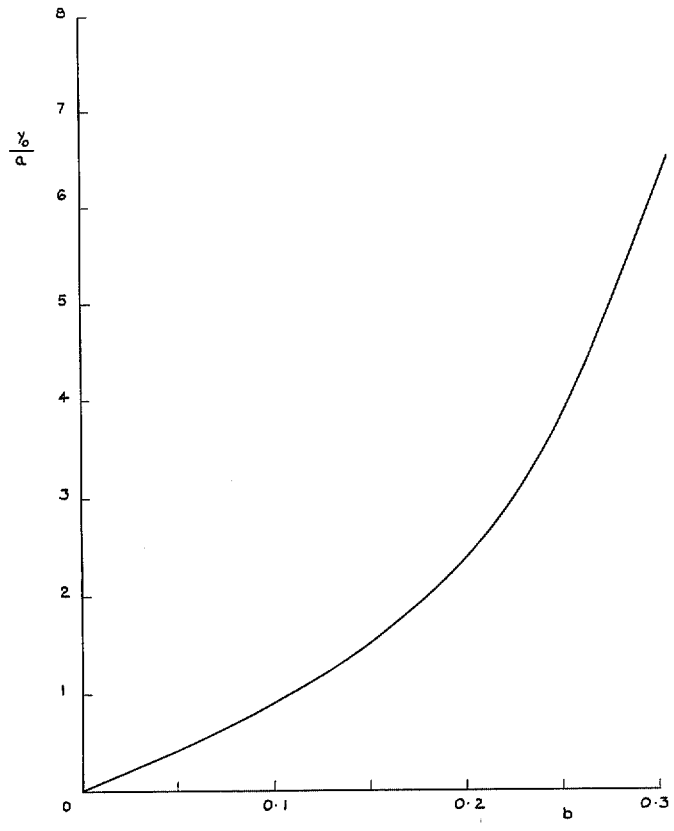

FIG. 5. Graph of $\frac{y_0}{a}$ against b.

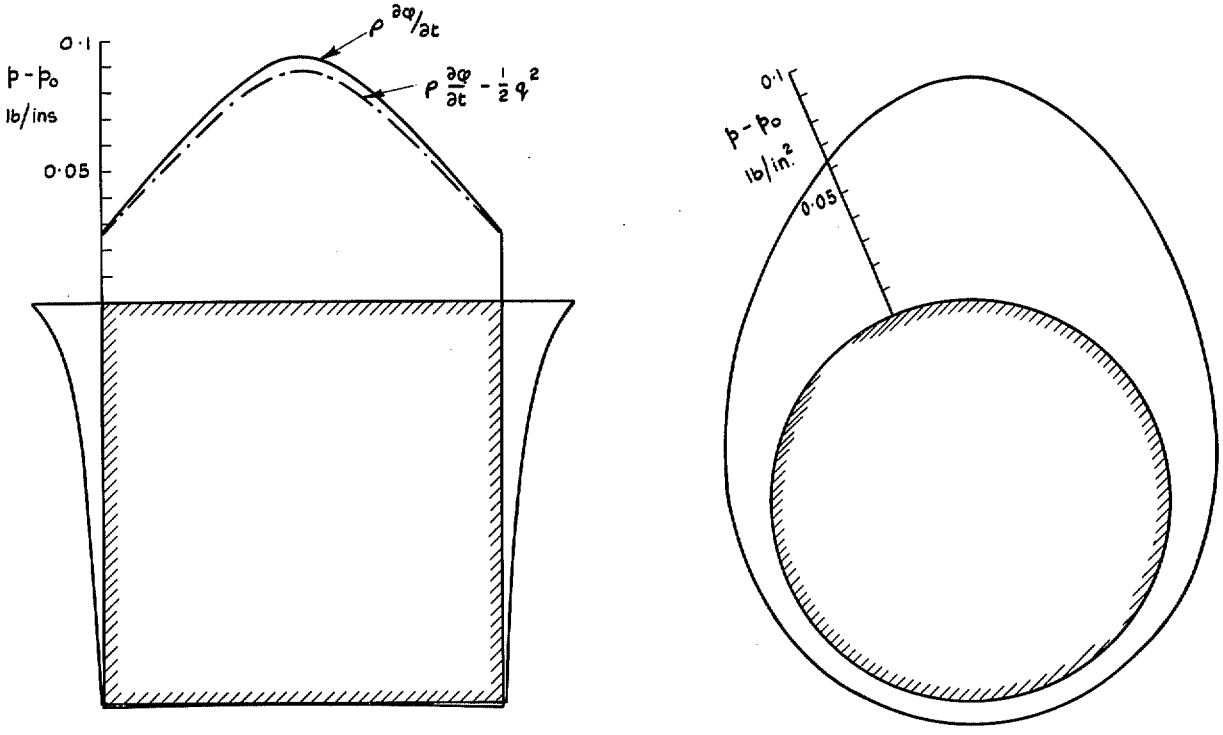

FIG. 6. Pressure distributions around square and circular fuselages.

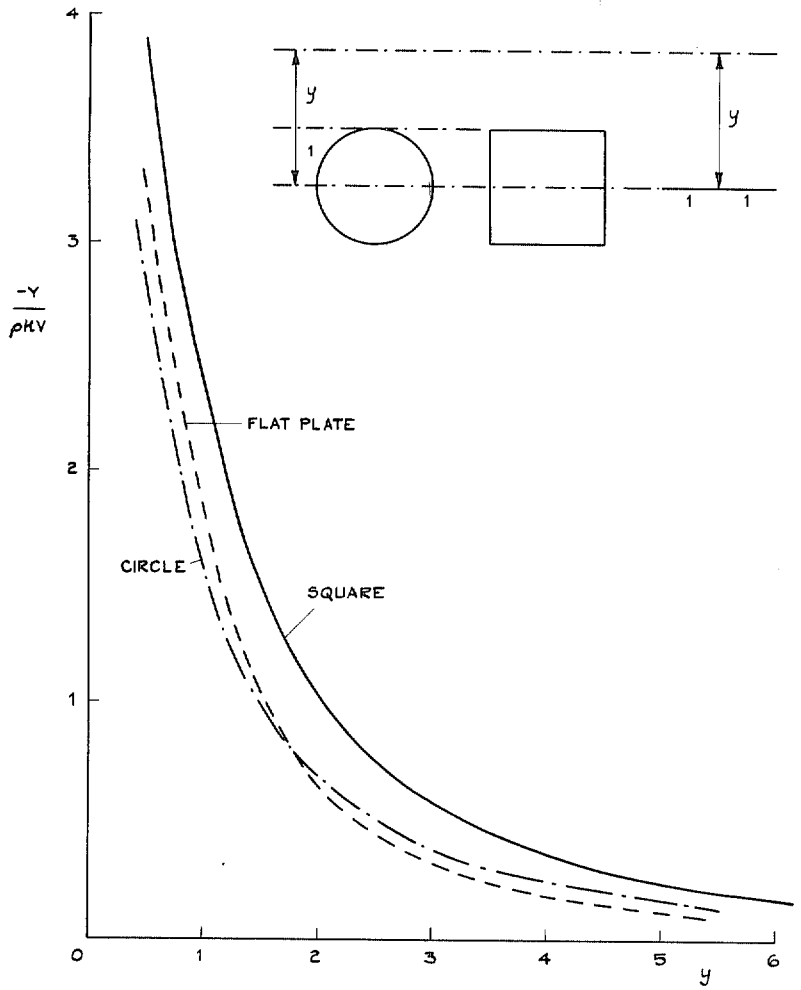

FIG. 7. Downward force on square and circular fuselages and flat-plate.

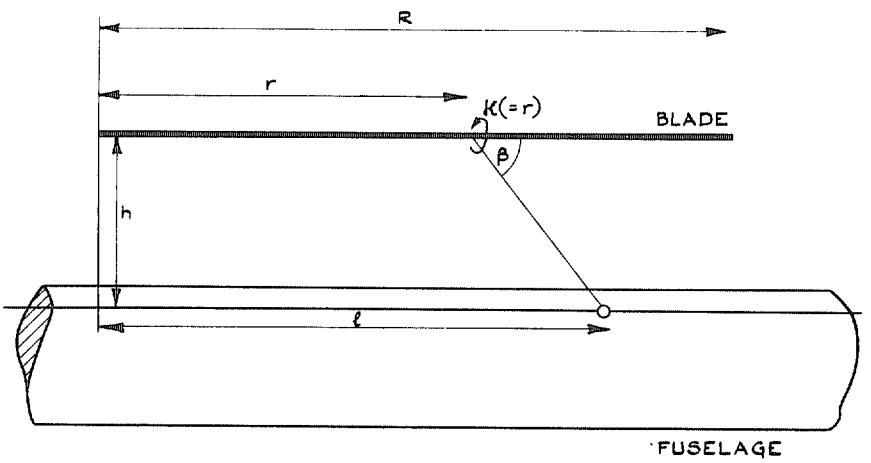

FIG. 8. Definition of quantities used in calculating end effect.

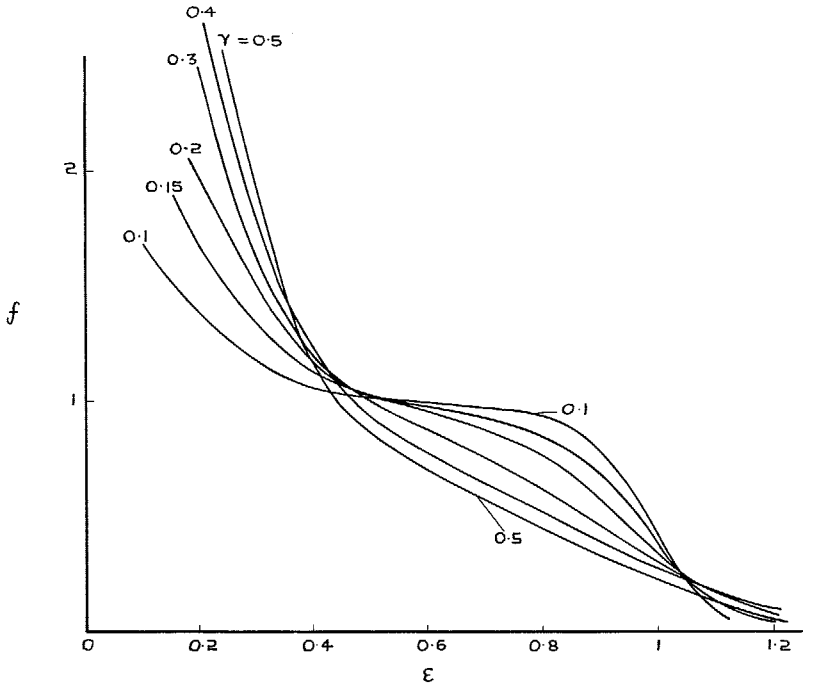

FIG. 9. Values of factor f for correcting two-dimensional pressure distributions.

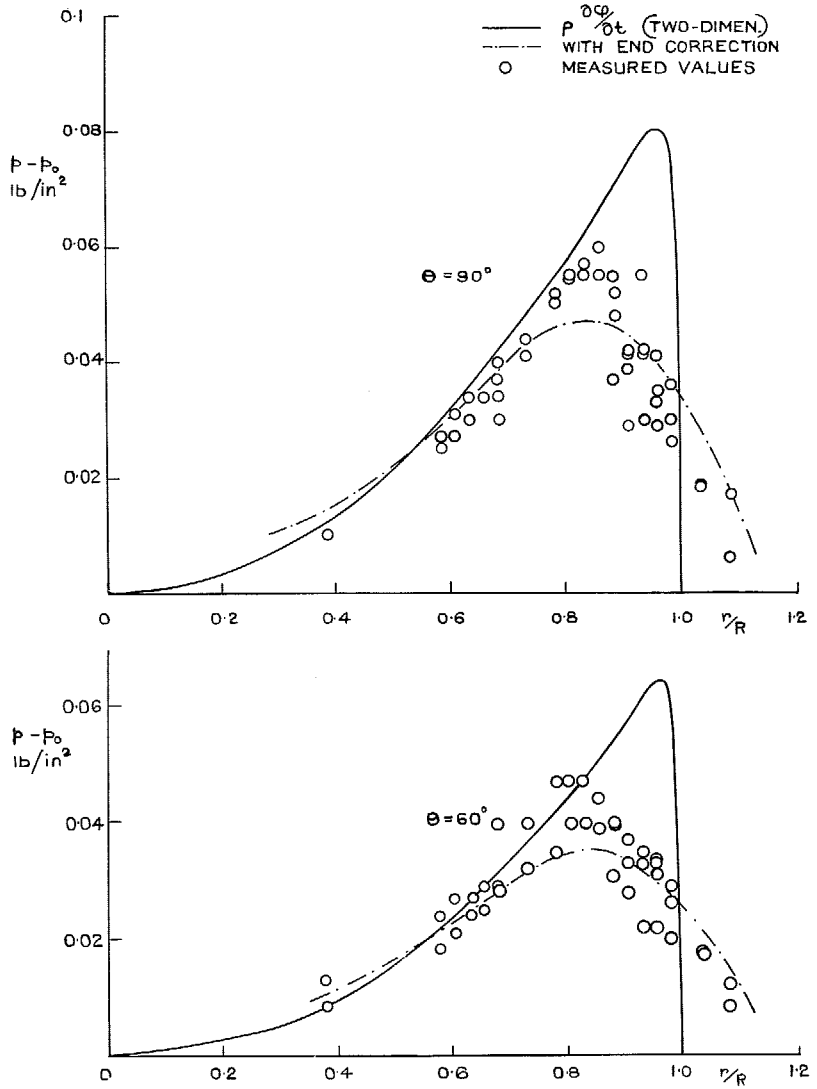

FIG. 10. Application of end effect to two-dimensional theory shown in Fig. 2 and comparison with measured values.

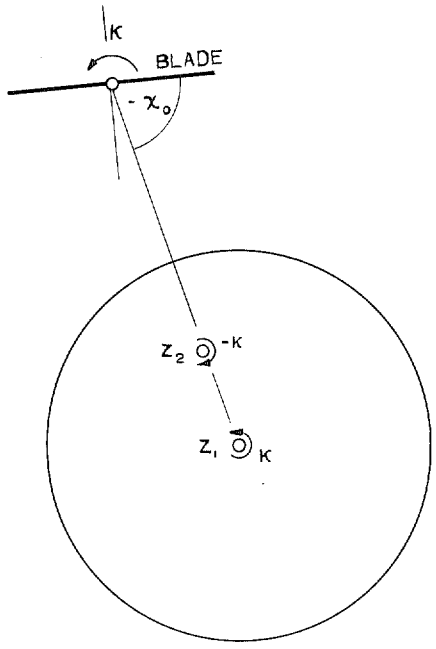

FIG. 11. Image system for calculating forces on blade.

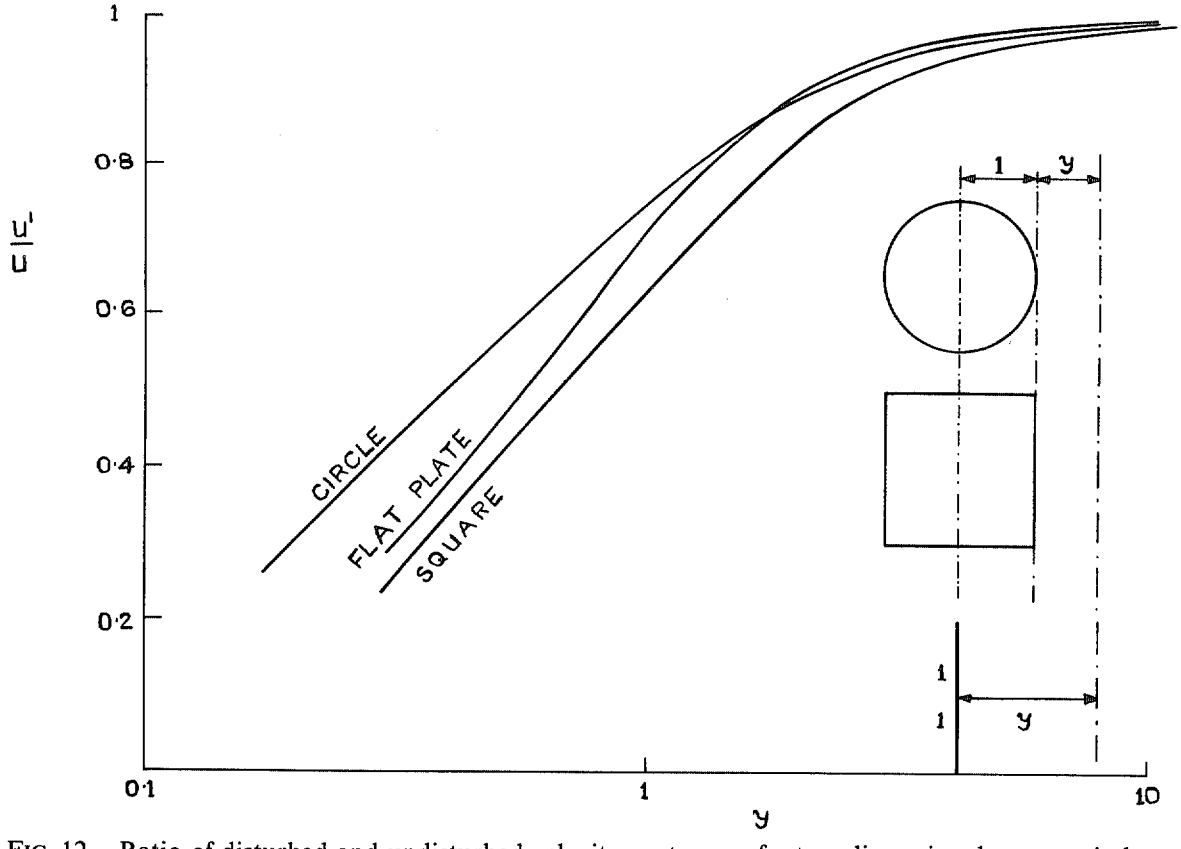

FIG. 12. Ratio of disturbed and undisturbed velocity upstream of a two-dimensional square, circle or flat plate in a uniform stream.

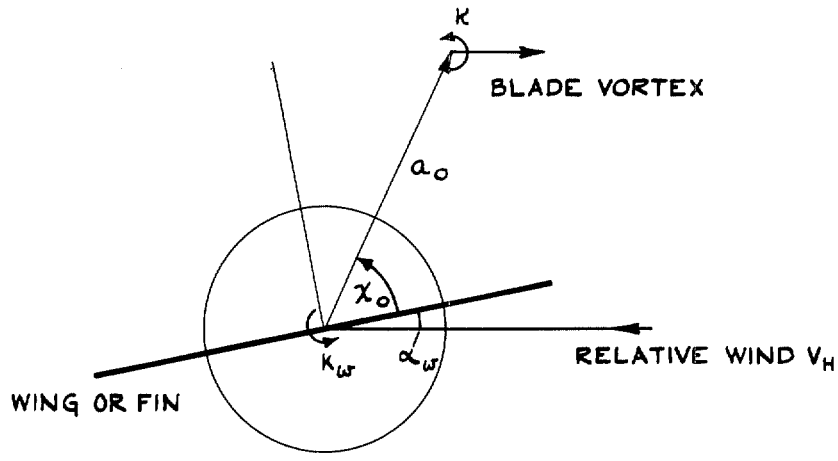

FIG. 13a. Mathematical model used for calculating flow about a wing or fin.

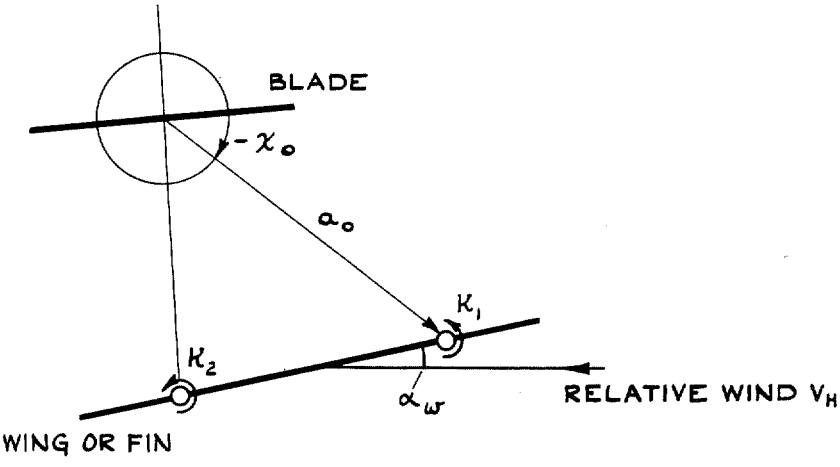

FIG. 13b. Mathematical model used for calculating time-dependent pressures on a blade.

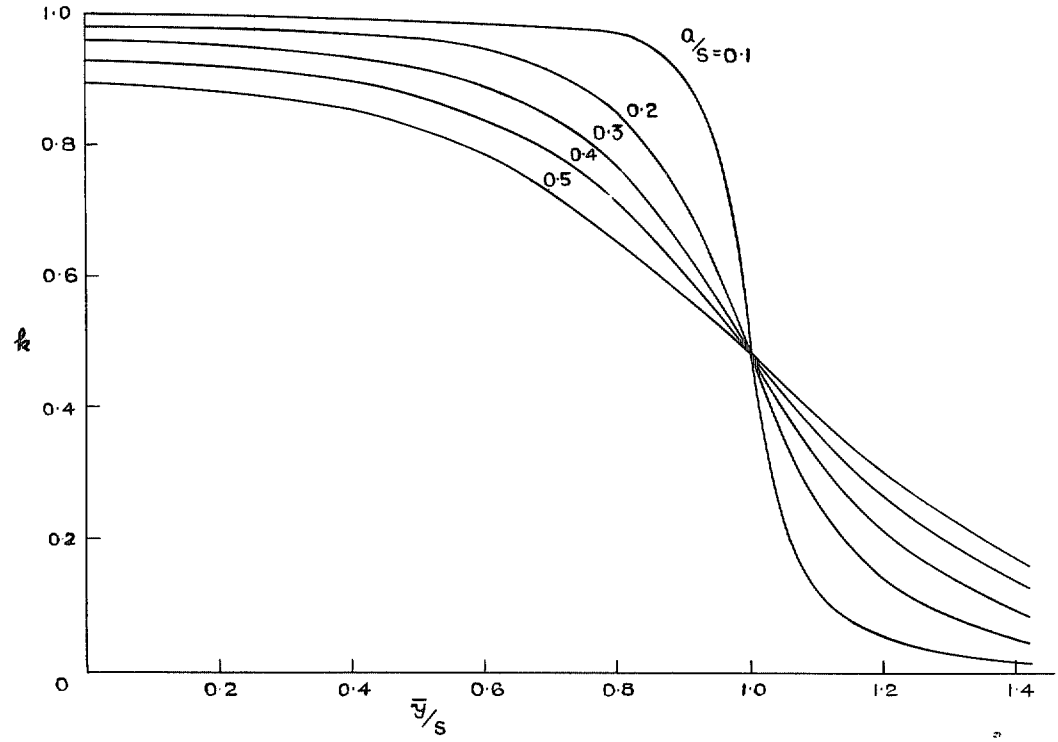

FIG. 14. Factor for applying 'end correction' to two-dimensional calculations of interference from uniformly-loaded wing.

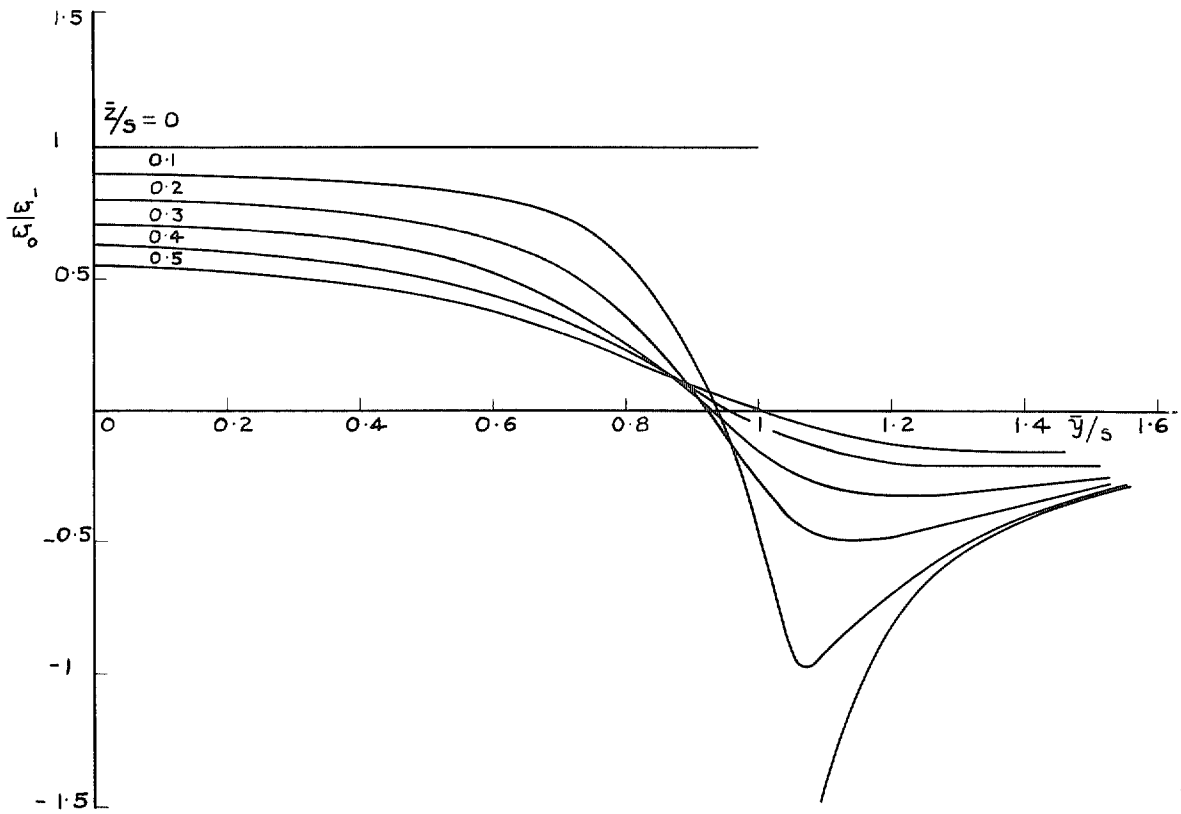

FIG. 15. Variation of normal induced velocity in lateral plane.

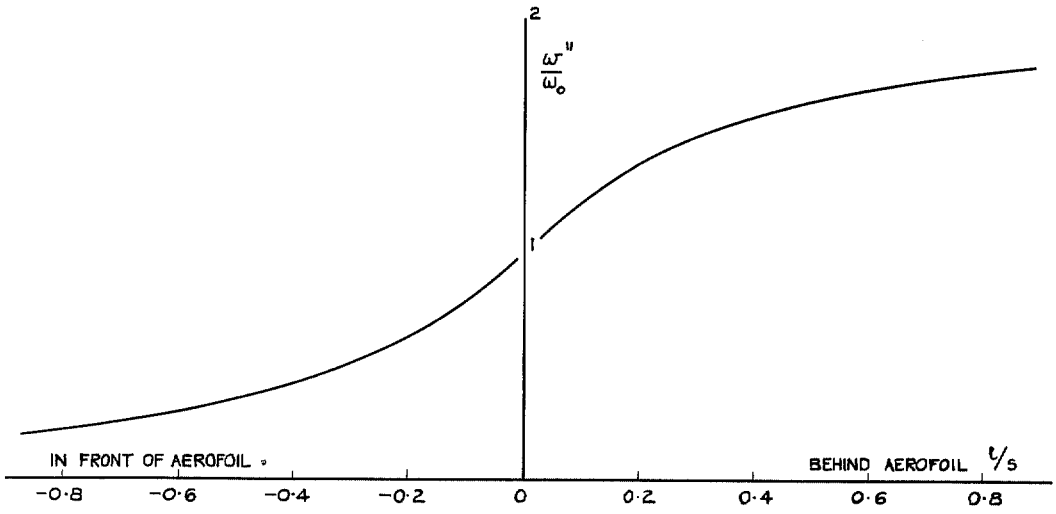

FIG. 16. Variation of normal induced velocity along longitudinal axis of symmetry.

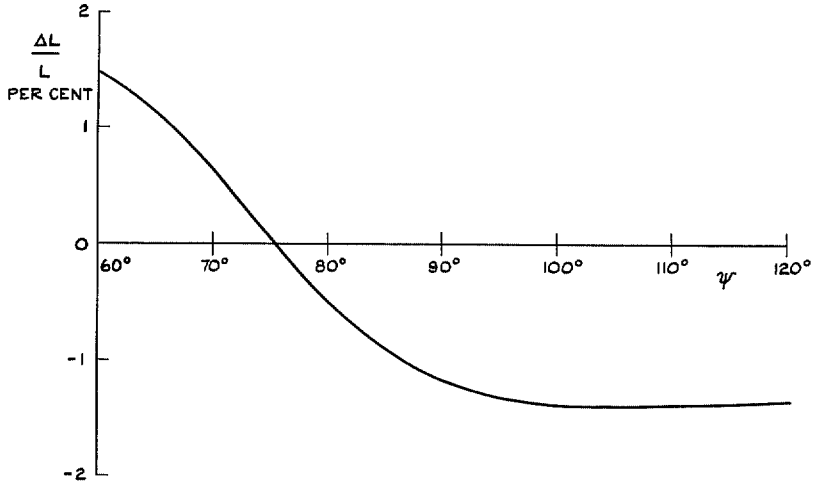

FIG. 17a. Variation of lift near tip of 'Rotodyne' wing due to passage of advancing blade ($\mu = 0{\cdot}35$, $\frac{r}{R} = 0{\cdot}5$)

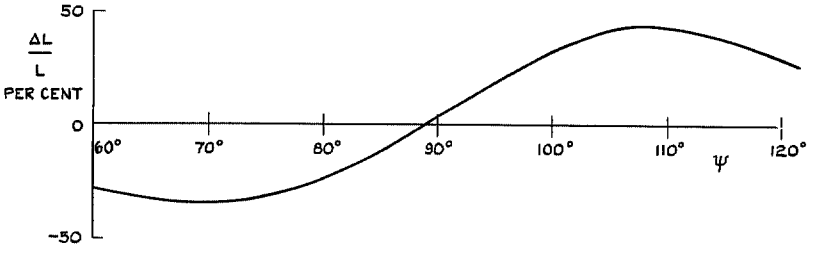

FIG. 17b. Variation of lift on advancing 'Rotodyne' blade. ($\mu = 0{\cdot}35$, $\frac{r}{R} = 0{\cdot}5$)

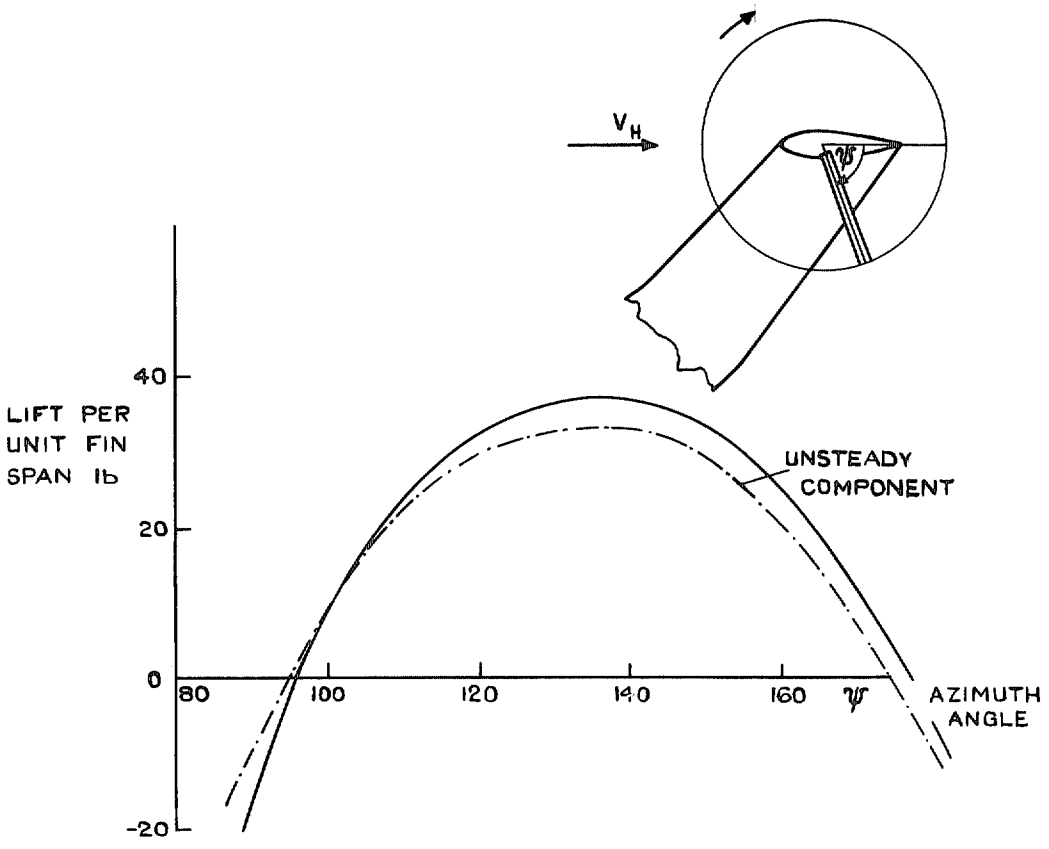

FIG. 18a. Variation of fin lift due to passage of tail rotor blade.

(Westland 'Wessex', $V_H = 170$ ft/sec, $\frac{r}{R} = 0{\cdot}75$)

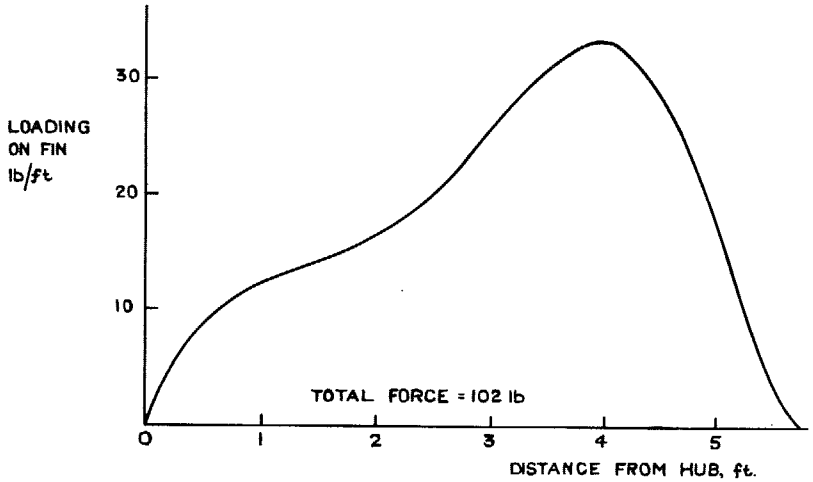

FIG. 18b. Maximum loading on 'Wessex' tail-fin in hovering flight ($\psi = 135$ deg, blade $C_L = 0{\cdot}41$, $\Omega R = 710$ ft/sec)

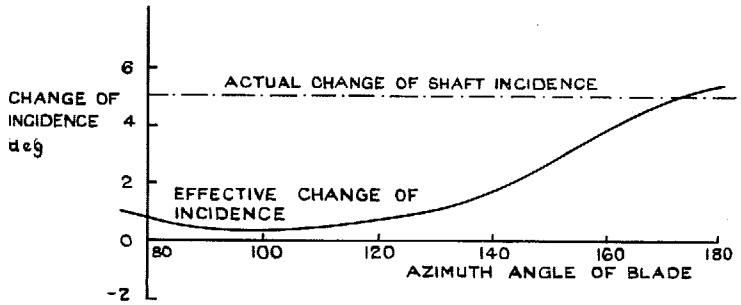

FIG. 18c. Effective change of incidence of shaft felt at blade compared with actual change of shaft incidence. (Blade 1·4 ft from fin, fin chord = 4 ft.).

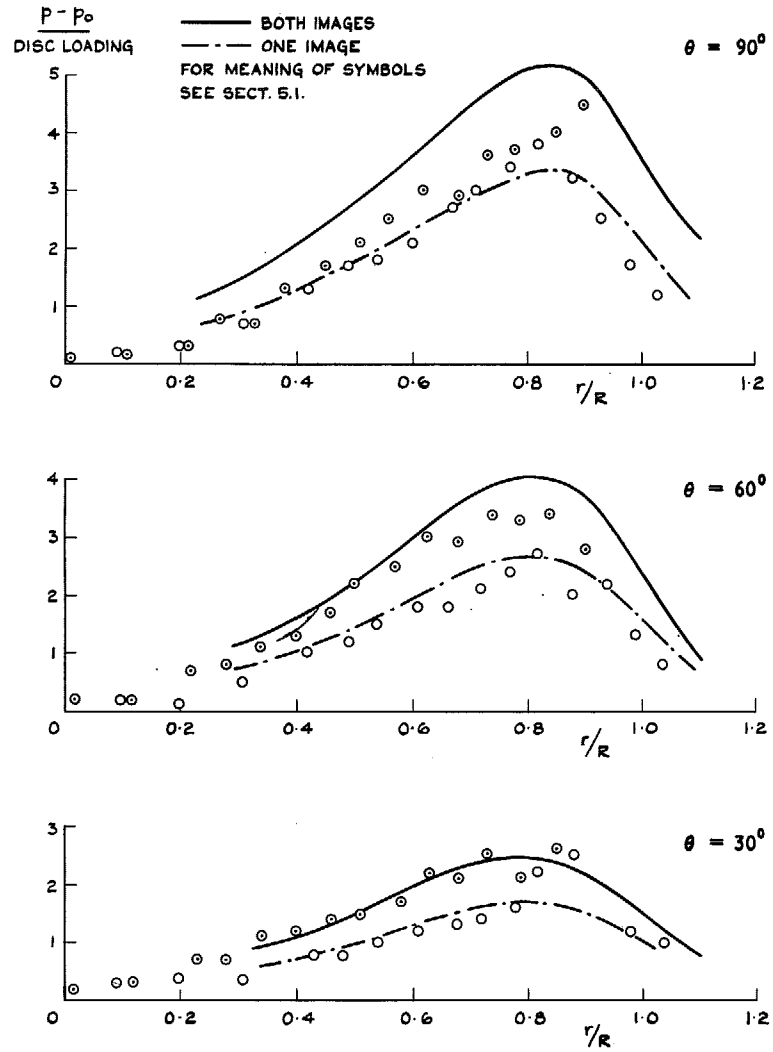

FIG. 19. Comparison of theory with NASA cylinder tests. ($c = 0{\cdot}33$ ft, $\alpha = 0{\cdot}5$ ft, $\alpha_0 = 0{\cdot}83$ ft, $\Omega R = 367$ ft/sec).

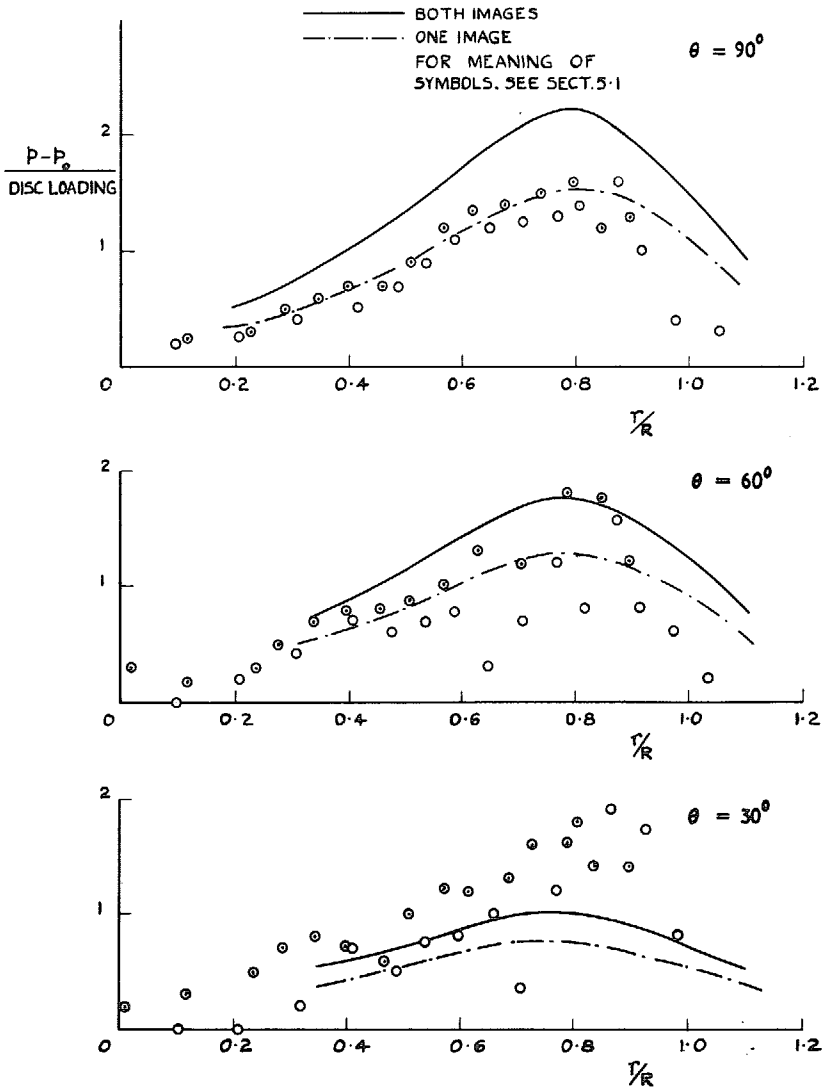

FIG. 20. Comparison of theory with NASA cylinder tests. ($c = 0{\cdot}33$ ft, $\alpha = 0{\cdot}5$ ft, $\alpha_0 = 1{\cdot}17$ ft, $\Omega R = 367$ ft/sec).

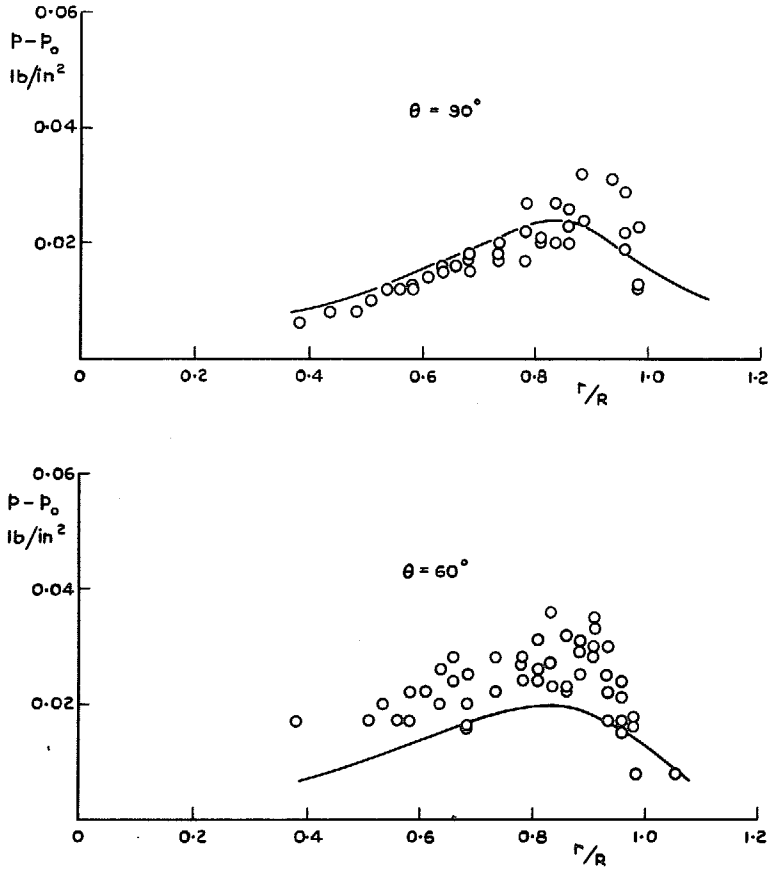

FIG. 21. Comparison of theory with R.A.E. cylinder tests. $c = 0{\cdot}5$ ft, $\alpha = 0{\cdot}5$ ft, $\alpha_0 = 1{\cdot}5$ ft, $\Omega R = 357$ ft/sec.

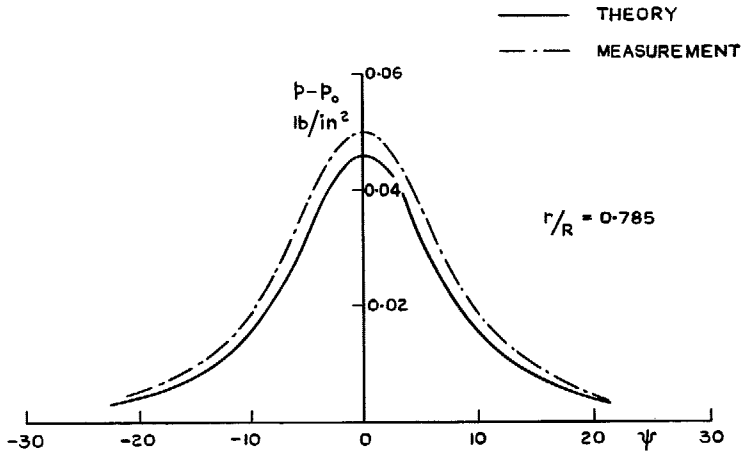

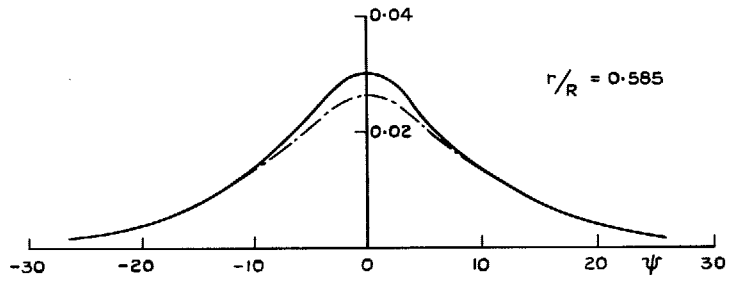

FIG. 22. Variation of presure on top of circular fuselage with azimuth angle of blade. (Conditions same as for Fig. 2).

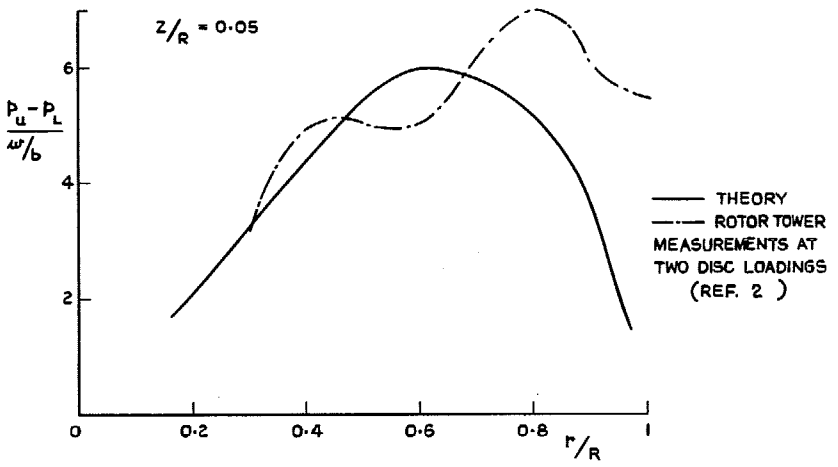

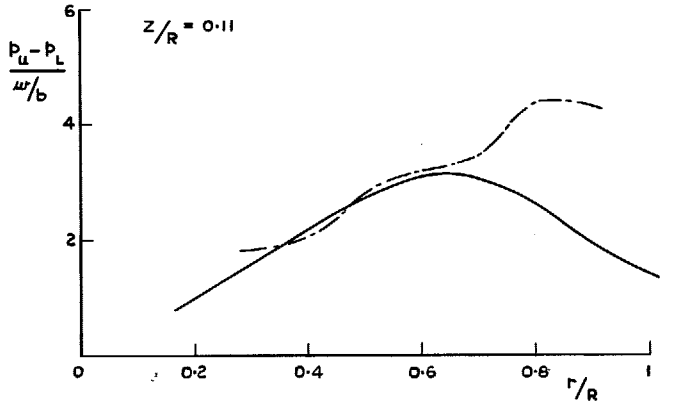

FIG. 23. Comparison of NASA pressure measurements on a flat panel with theory.

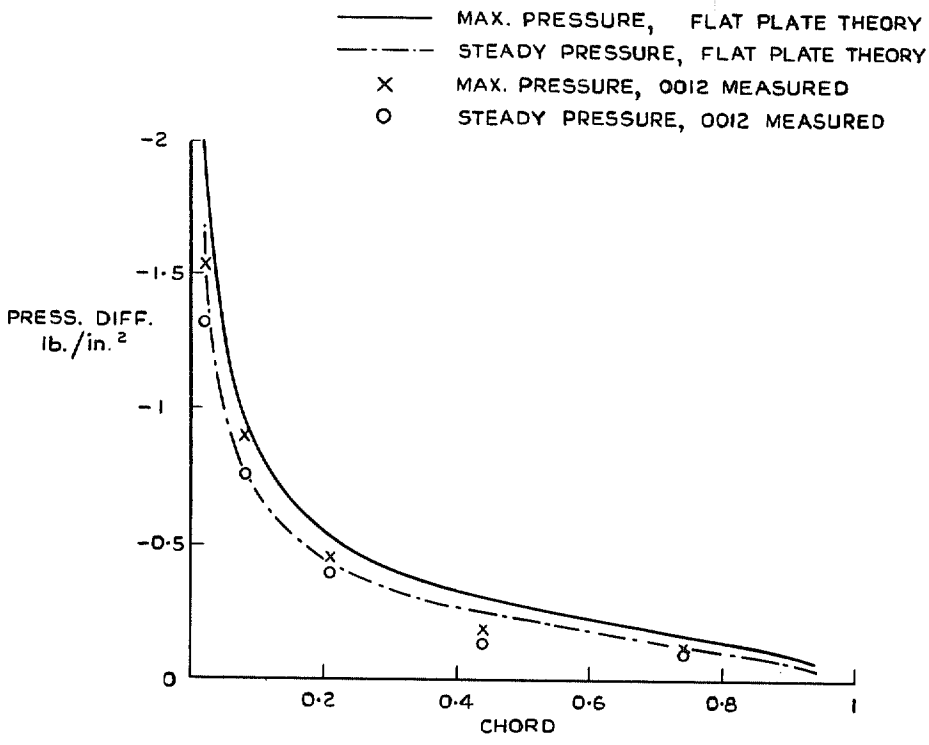

FIG. 24. Maximum and steady pressures on a flat-plate aerofoil with measurements on a NASA 0012 aerofoil for comparison. (Same conditions as Fig. 2).

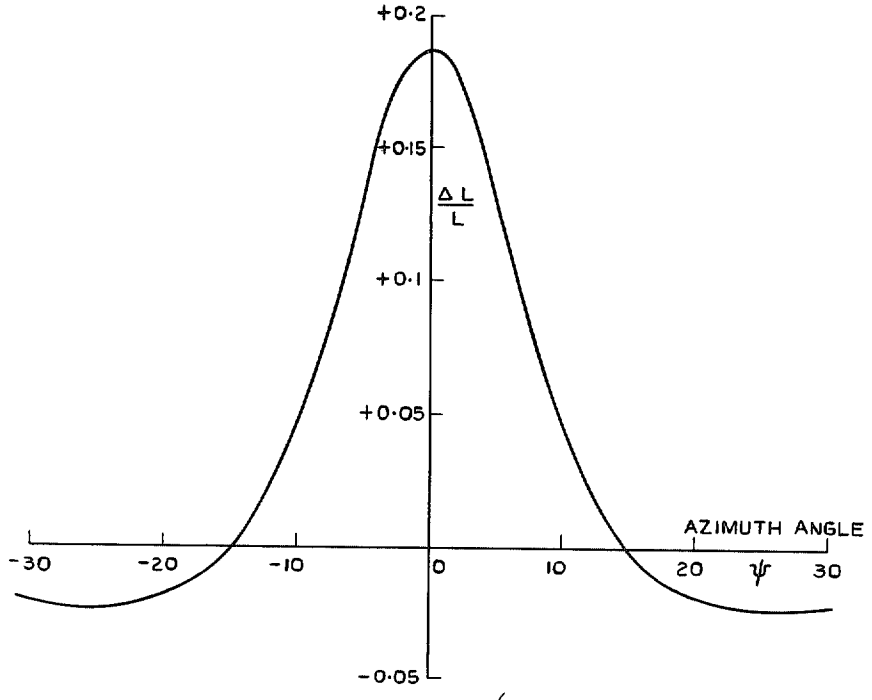

FIG. 25. Variation of blade lift with azimuth angle. $\left(\frac{r}{R} = 0{\cdot}8, \Phi = 5 \text{ deg}, \alpha = 5 \text{ deg}, \kappa = 0{\cdot}435\right)$

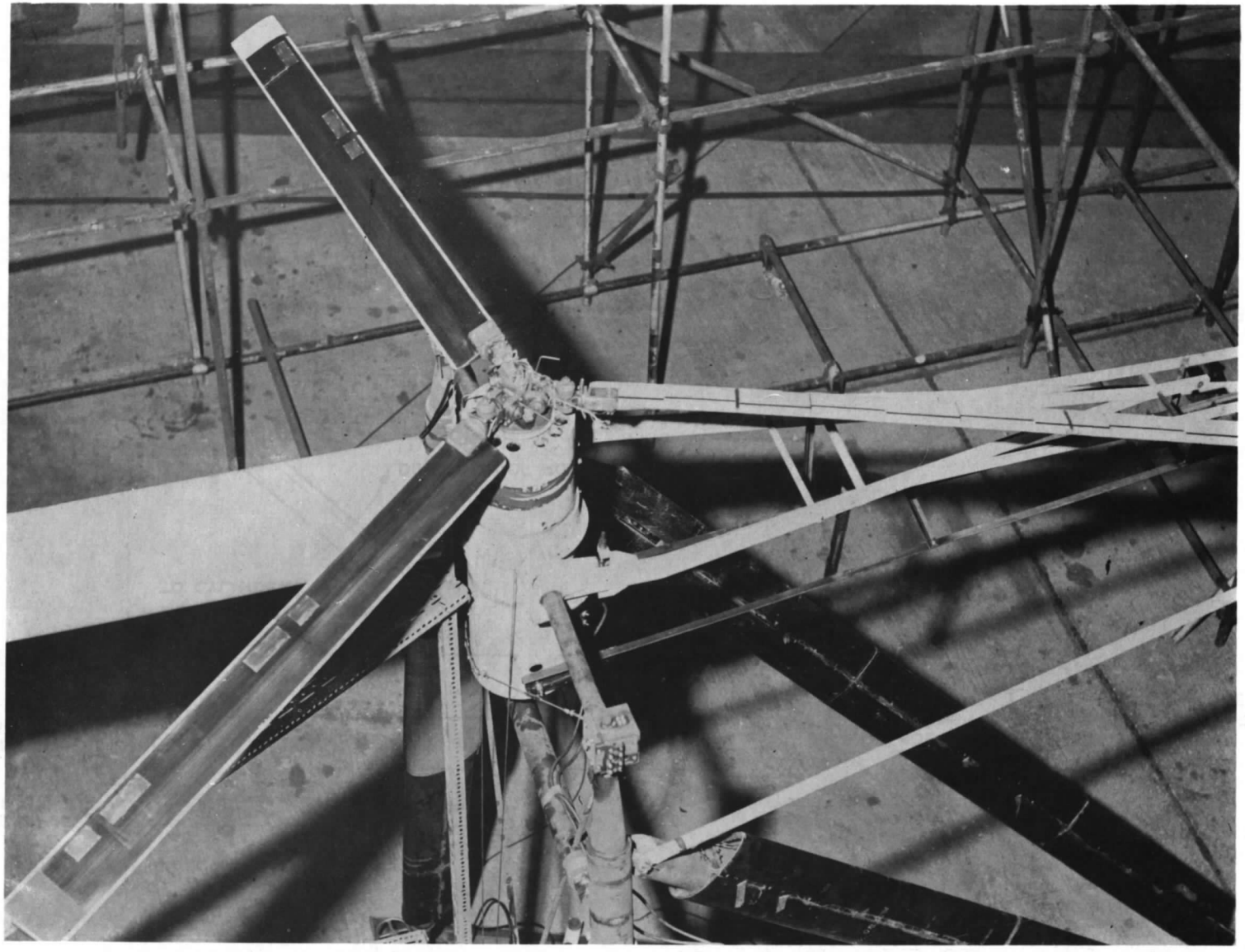

FIG. 26. General view of cylinder beneath hovering rotor.

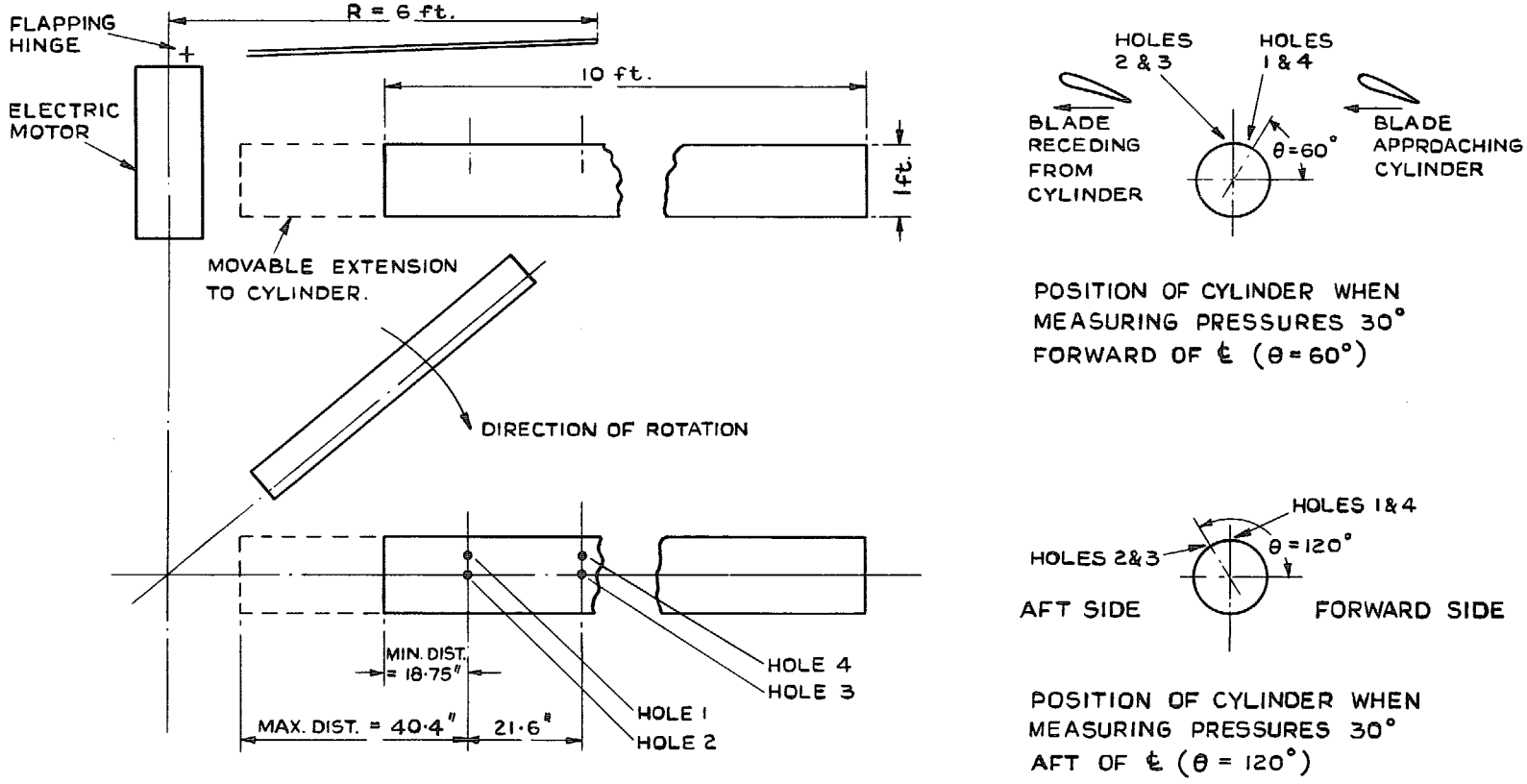

FIG. 27. Details of cylinder and pressure hole positions.

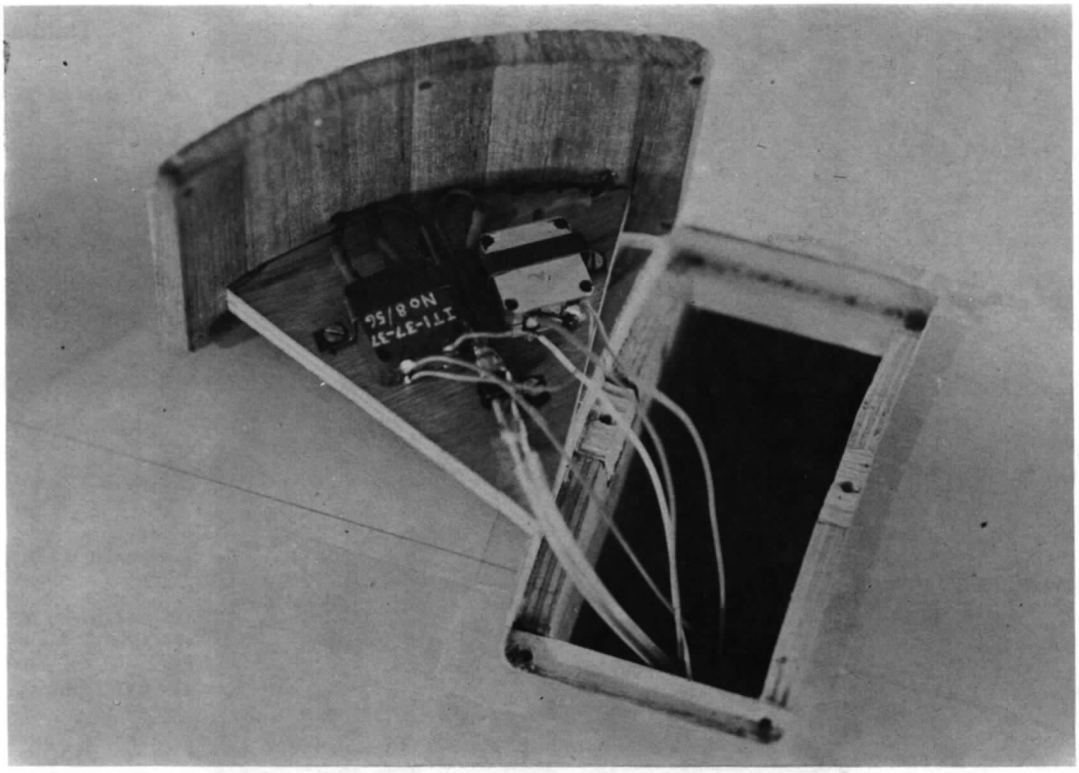

FIG. 28. Pressure transducers installed in cylinder.

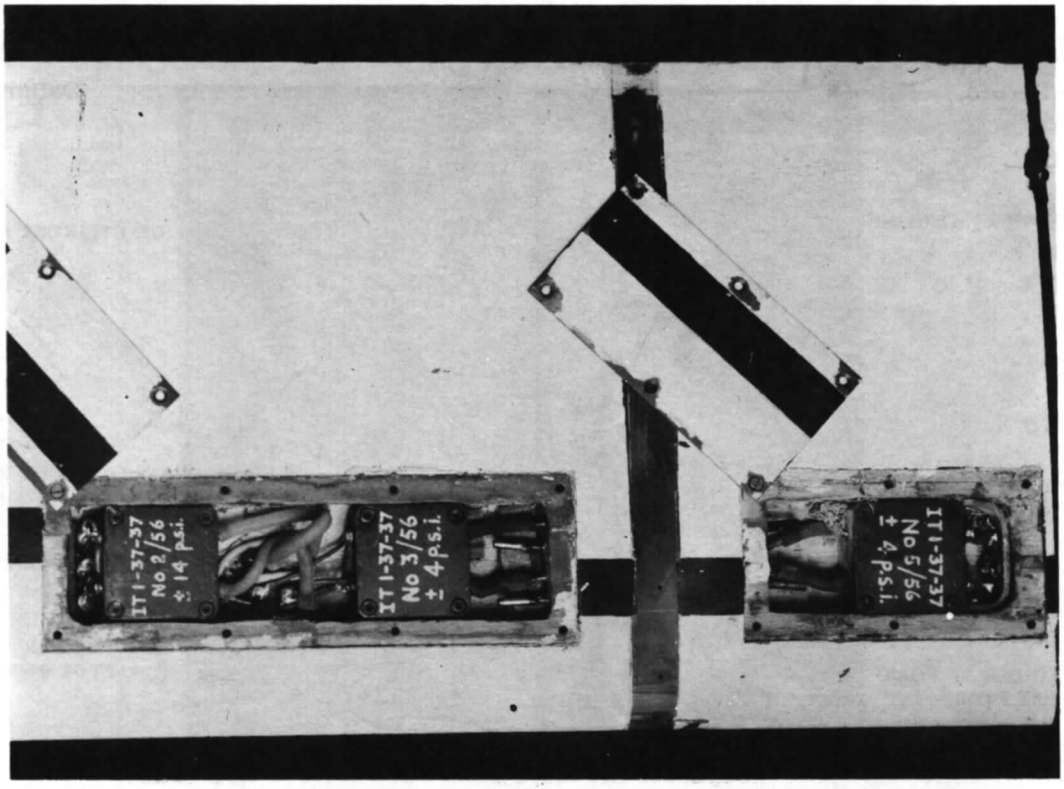

FIG. 29. Pressure transducers installed in blade.

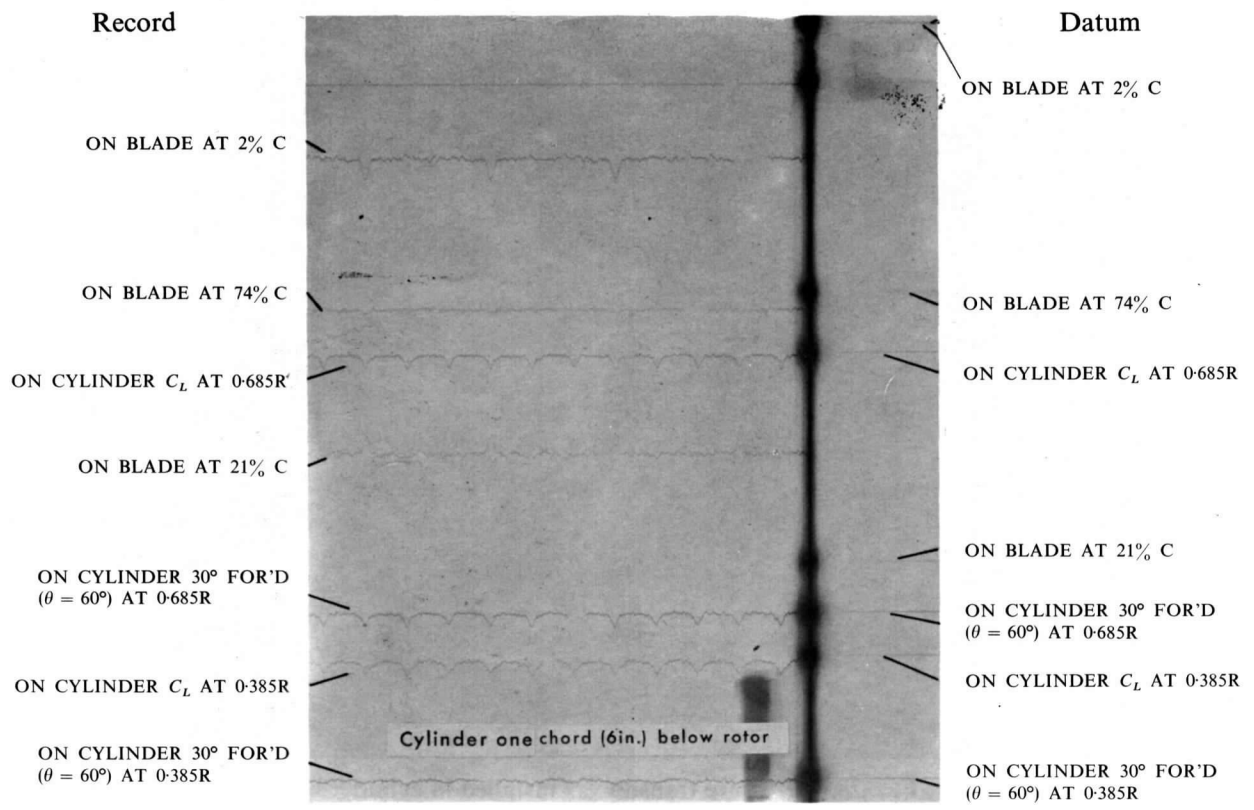

FIG. 30. Typical galvanometer traces obtained from pressure transducers.

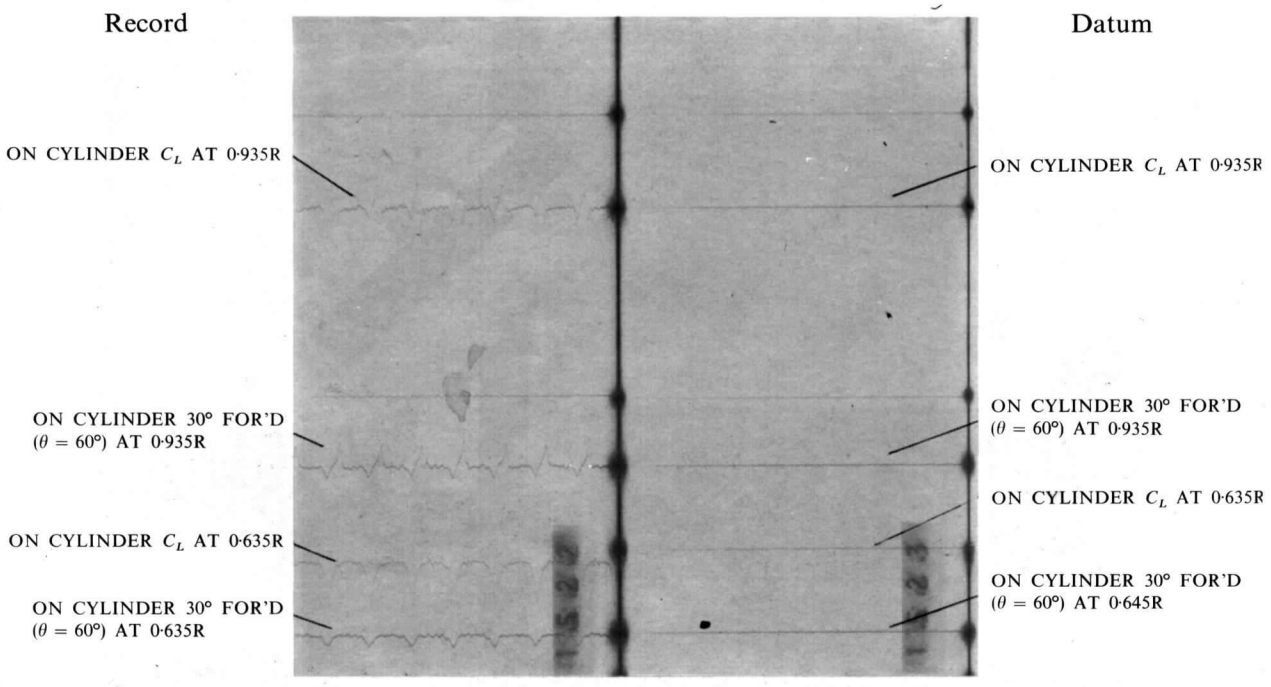

Cylinder one chord (6 in.) below rotor

FIG. 30 (contd.). Typical galvanometer traces obtained from pressure transducers.

Printed in Wales for Her Majesty's Stationery Office by Allens Printers (Wales) Limited

Dd.129527 K 5

Published by
HER MAJESTY'S STATIONERY OFFICE

To be purchased from
49 High Holborn, London W.C.1
423 Oxford Street, London W.1
13A Castle Street, Edinburgh 2
109 St. Mary Street, Cardiff, CF1 1JW
Brazennose Street, Manchester 2
50 Fairfax Street, Bristol 1
258–259 Broad Street, Birmingham 1
7–11 Linenhall Street, Belfast, BT2 8AY
or through any bookseller

S.O. Code No. 23–[illegible]